Corner Singularities for the Fractional Laplacian and Finite Element Approximation

Heiko Gimperlein*† Ernst P. Stephan‡ Jakub Stocek*

Abstract

Solutions to elliptic boundary value problems in polygonal domains exhibit singularities at edges and corners. In this article we consider the integral fractional Laplacian in polygonal domains and discuss the regularity properties and numerical approximation of solutions. We study the detailed asymptotic expansions of the solution at edges and vertices. The vertex singularities are governed by an eigenvalue problem for a perturbed Laplace-Beltrami operator on the upper hemisphere. Its analysis and numerical approximation generalize classical results for screen problems for the standard Laplace equation. Our results imply quasi-optimal convergence rates for the approximation by h-version finite elements on graded meshes. Numerical experiments illustrate the theory and provide numerical tables for the singular vertex exponents, depending on the geometry of the domain and the order of the operator.

1 Introduction

For solutions to elliptic equations in a polyhedral domain, the asymptotic behavior near the edges and corners has been studied for several decades [10, 21, 25, 26]. Numerically, the explicit singular expansions allow to recover optimal convergence rates for finite [4, 5] and boundary element methods [30, 31].

Recently, there has been much interest in boundary problems for nonlocal operators such as the fractional Laplacian [8, 22] and their numerical approximation [1, 2, 3, 11]. The integral fractional Laplacian $(-\Delta)^s$ in a domain $\Omega \subset \mathbb{R}^n$ arises, for instance, in the pricing of stock options [35], image processing [19], continuum mechanics [13], and in the movement of biological organisms [14] and swarm robotic systems [15].

Sharp results for the regularity of the solutions to such problems in smooth domains have been obtained by Grubb [22], and for $C^{1,\alpha}$ domains by Ros-Oton and Serra [33]. A recent alternative approach is given in [17]. In convex polygons, weighted Sobolev estimates were shown in [2], resulting in optimal convergence rates on graded meshes. Regularity results have also been obtained for operators like the spectral fractional Laplacian, with applications to the convergence of *hp* discretisations in analytic domains [7].

*Maxwell Institute for Mathematical Sciences and Department of Mathematics, Heriot–Watt University, Edinburgh, EH14 4AS, United Kingdom, email: h.gimperlein@hw.ac.uk.

†Institute for Mathematics, University of Paderborn, Warburger Str. 100, 33098 Paderborn, Germany.

J. S. was supported by The Maxwell Institute Graduate School in Analysis and its Applications, a Centre for Doctoral Training funded by the UK Engineering and Physical Sciences Research Council (grant EP/L016508/01), the Scottish Funding Council, Heriot-Watt University and the University of Edinburgh.

‡Institute of Applied Mathematics, Leibniz University Hannover, 30167 Hannover, Germany

In this article we consider the fractional Dirichlet problem in a polygon Ω,

$$\begin{aligned} (-\Delta)^s u &= f \text{ in } \Omega, \\ u &= 0 \text{ in } \Omega^C = \mathbb{R}^2 \setminus \overline{\Omega}, \end{aligned} \tag{1}$$

where $s \in (0,1)$. For $s = \frac{1}{2}$ and $s = 1$ the problem has a long history: the Dirichlet problem for the Laplacian in Ω when $s = 1$, the hypersingular integral equation $Wu = 2f$ on the flat screen $\Omega \times \{0\} \subset \mathbb{R}^3$ when $s = \frac{1}{2}$.

We obtain precise asymptotic expansions for the solution u of (1) near the boundary and corners for all $s \in (0,1)$. These expansions allow us to prove optimal convergence rates for the h-version finite element method on algebraically graded meshes. Our results generalize classical results for the Laplace equation in polygons and its numerical approximation by finite and boundary element methods.

The results of Grubb [22] show that near a smooth boundary $\frac{u}{\operatorname{dist}(x,\partial\Omega)^\nu}$ is smooth up to $\partial\Omega$ with leading singular exponent $\nu = s$. We obtain a similar asymptotic behavior in a corner. There the leading singular exponent λ is determined by a spectral problem for a perturbation of the Laplace-Beltrami operator on the upper hemisphere with mixed boundary conditions. This exponent λ is an increasing function of s and a decreasing function of the corner angle. The upper and lower bounds $\lambda < 2s$, $\lambda > \max\{0, s - \frac{1}{2}\}$, are sharp. Generalizing [27, 34] for $s = \frac{1}{2}$, we numerically approximate the eigenvalue problem for λ to study its behavior in s and the corner angle. The appendix derives an accurate analytical approximation for λ.

The precise asymptotic description of the solution has implications for the approximation by finite elements. We consider the best approximation of u by piecewise polynomial functions $\mathbb{V}_h$ on a β-graded mesh, graded towards the boundary and the corners. A main result recovers optimal convergence rates for general polygonal domains:

Theorem. Let $u \in \widetilde{H}^s(\Omega)$ be the solution to the continuous problem, $U_h \in \mathbb{V}_h$ the best approximation to u on a β-graded mesh. Then

$$\|u - U_h\|_{\widetilde{H}^s(\Omega)} \lesssim h^{\min\{\frac{\beta}{2}, 2-s\}-\varepsilon} .$$

This generalizes the results of [2]. In 2d, the approximation rate is therefore determined by the boundary behavior $\nu = s$ of the solution, and independent of the corner exponent λ.

For the numerical approximation λ_h of λ we similarly obtain:

Corollary. Let λ_h be the approximation to λ obtained from the finite element approximation of the lowest eigenvalue to the spectral problem on a β–graded mesh with $\beta > \frac{2-s}{\nu(s)+\frac{1}{2}-s}$. Then for $\varepsilon > 0$,

$$|\lambda_h - \lambda| \leq C_{\beta,\varepsilon} h^{2\min\{\beta s, 2-s\}-\varepsilon}$$

For a discretization on a quasi-uniform mesh,

$$|\lambda_h - \lambda| \leq C_{\beta,\varepsilon} h^{2s}.$$

Numerical experiments based on a finite element discretization of (1) confirm the theoretical results for the singular exponents ν, λ and achieve the predicted convergence rates. In particular, the convergence rate for the solution u in the energy space $\widetilde{H}^s(\Omega)$ is doubled on a 2-graded mesh, when compared to a uniform mesh.

We also determine the corner exponents λ numerically, by determining the lowest eigenvalue of the spectral problem on the upper hemisphere. As for u, the convergence rate for λ confirms the theoretical predictions. Furthermore, we compute λ empirically from the asymptotic behavior of the finite element solutions near corner points, as well as from the analytical approximation in the appendix. The different approximations agree quantitatively for all s and all corner angles and confirm the qualitative predictions. For a corner of opening angle approaching 2π, λ approaches the analytical lower bound $\max\{0, s-\frac{1}{2}\}$. A table for λ as a function of s and the corner angle is provided, generalising the classical table of [27] for $s=\frac{1}{2}$.

Structure of this article: Section 2 recalls definitions and notation related to the integral fractional Laplacian and the relevant Sobolev spaces. The fractional Dirichlet problem and its weak formulation are discussed in Section 3. Section 4 reformulates the Dirichlet problem as a degenerately elliptic differential boundary problem in one dimension higher, with mixed boundary conditions. The asymptotic expansion and approximation properties of the solution are introduced in Section 5. The proof of the approximation results is then presented in Section 6. Section 7 discusses the numerical approximation of the corner exponent, based on a finite element discretization of the appropriate spectral problem. The following Section 8 discusses algorithmic details of the implementation. The article concludes with numerical experiments in Section 9. Appendix 10 contains an analytic approximation of the corner exponent.

2 Sobolev spaces and the fractional Laplacian

We recall basic definitions and properties related to Sobolev spaces of non-integer order and to the fractional Laplacian. For further details we refer to [12].
Let $\Omega \subset \mathbb{R}^n$ be a bounded domain, and for $s \in \mathbb{N}_0$, $H^s(\Omega)$ the Sobolev space of functions in $L^2(\Omega)$ whose distributional derivatives of order s belong to $L^2(\Omega)$. For $s \in (0,\infty)$, we write $m = \lfloor s \rfloor$ and $\sigma = s - m$ and define the Sobolev space $H^s(\Omega)$ as

$$H^s(\Omega) = \{v \in H^m(\Omega) : |\partial^\alpha v|_{H^\sigma(\Omega)} < \infty \quad \forall |\alpha| = m\} \ .$$

Here $|\cdot|_{H^\sigma(\Omega)}$ is the Aronszajn-Slobodeckij seminorm

$$|v|^2_{H^\sigma(\Omega)} = \iint_{\Omega\times\Omega} \frac{(v(x)-v(y))^2}{|x-y|^{n+2\sigma}} \,\mathrm{d}y\,\mathrm{d}x.$$

$H^s(\Omega)$ is a Hilbert space endowed with the norm

$$\|v\|^2_{H^s(\Omega)} = \|v\|^2_{H^m(\Omega)} + \sum_{|\alpha|=m} |\partial^\alpha v|^2_{H^\sigma(\Omega)}.$$

Particularly relevant for this article is the space

$$\widetilde{H}^s(\Omega) = \{v \in H^s(\mathbb{R}^n) : \operatorname{supp} v \subset \overline{\Omega}\}$$

of distributions whose extension by 0 belongs to $H^s(\mathbb{R}^n)$.

We recall that when Ω is Lipschitz and $\frac{1}{2} \neq s \in (0,1)$, $\widetilde{H}^s(\Omega)$ coincides with the space $H^s_0(\Omega)$, which is the closure of $C^\infty_0(\Omega)$ with respect to the H^s norm. Moreover, for $s \in (0, \frac{1}{2})$, $\widetilde{H}^s(\Omega) = H^s(\Omega) = H^s_0(\Omega)$. All three spaces differ when $s = \frac{1}{2}$.

For negative s the Sobolev spaces are defined by duality.

For $s \in (0,1)$, we define the fractional Laplacian of a Schwartz function u on $\mathbb{R}^n$ by

$$(-\Delta)^s u(X) = c_{n,s}\, P.V. \int_{\mathbb{R}^n} \frac{u(X)-u(Y)}{|X-Y|^{n+2s}} \,\mathrm{d}Y = c_{n,s} \lim_{\varepsilon\to 0^+} \int_{\mathbb{R}^n\setminus\overline{\mathcal{B}}_\varepsilon(X)} \frac{u(X)-u(Y)}{|X-Y|^{n+2s}} \,\mathrm{d}Y \ , \quad (2)$$

where *P.V.* denotes the Cauchy principal value and $\mathcal{B}_\varepsilon(X)$ the n-dimensional ball of radius $\varepsilon > 0$ centered at X. The normalization constant $c_{n,s}$ is defined in terms of Γ functions:

$$c_{n,s} = \frac{2^{2s} s \Gamma\left(\frac{n+2s}{2}\right)}{\pi^{\frac{n}{2}} \Gamma(1-s)}.$$

Equivalently, the fractional Laplacian may be defined in terms of the Fourier transform on $\mathbb{R}^n$ as $\mathcal{F}((-\Delta)^s u) = |\xi|^{2s} \mathcal{F}u$. This expression extends $(-\Delta)^s$ to an unbounded operator on $L^2(\mathbb{R}^n)$. It also shows that $(-\Delta)^s$ is an operator of order $2s$ and that for $s = 1$ one recovers the ordinary Laplace operator.

3 Dirichlet problem for fractional Laplacian in a domain

Let $\Omega \subset \mathbb{R}^n$ be a bounded Lipschitz domain and $f \in L^2(\Omega)$. The Dirichlet problem for the fractional Laplacian is formally given by:

$$\begin{aligned} (-\Delta)^s u &= f \qquad \text{in } \Omega, \\ u &= 0 \qquad \text{in } \mathbb{R}^n \setminus \overline{\Omega}. \end{aligned} \tag{3}$$

For $s \in (0,1)$, the weak form is expressed in terms of the bilinear form a on $\widetilde{H}^s(\Omega)$,

$$\mathsf{a}(u,v) = \frac{c_{n,s}}{2} \iint_D \frac{(u(X)-u(Y))(v(X)-v(Y))}{|X-Y|^{n+2s}} \,\mathrm{d}Y \,\mathrm{d}X \ , \tag{4}$$

where $D = (\mathbb{R}^n \times \Omega) \cup (\Omega \times \mathbb{R}^n)$.

Note that formally

$$\mathsf{a}(u,v) = \langle (-\Delta)^s u, v \rangle_{H^s(\mathbb{R}^n)} - \iint_{\Omega^c \times \Omega^c} \frac{(u(X)-u(Y))(v(X)-v(Y))}{|X-Y|^{n+2s}} \,\mathrm{d}Y \,\mathrm{d}X,$$

when $u, v \in H^s(\mathbb{R}^n)$, and the second term vanishes on $\widetilde{H}^s(\Omega)$. The weak form of (3) therefore reads as follows:

Find $u \in \widetilde{H}^s(\Omega)$ such that

$$\mathsf{a}(u,v) = \int_\Omega f v \,\mathrm{d}X, \tag{5}$$

for all $v \in \widetilde{H}^s(\Omega)$.

One verifies that a is continuous and elliptic in $\widetilde{H}^s(\Omega)$: There exist $C_\mathsf{a}, \alpha > 0$ with

$$\mathsf{a}(u,v) \le C_\mathsf{a} \|u\|_{\widetilde{H}^s(\Omega)} \|v\|_{\widetilde{H}^s(\Omega)}, \quad \mathsf{a}(u,u) \ge \alpha \|u\|^2_{\widetilde{H}^s(\Omega)} \ .$$

By Lax-Milgram, the weak form (5) admits a unique solution, and the solution operator $f \mapsto u$ extends to an isomorphism from $H^{-s}(\Omega)$ to $\widetilde{H}^s(\Omega)$.

4 Extension Problem

Following [8] for $\mathbb{R}^n$, resp. [17] for Ω, we introduce a boundary value problem for a degenerate partial differential operator in the half space $\mathbb{R}^n \times \mathbb{R}_+$, which is equivalent to (3):

$$L_s U(X,t) := t^{-\alpha} \nabla \cdot (t^\alpha \nabla U(X,t)) = \partial_t^2 U + \frac{1-2s}{t} \partial_t U + \Delta_X u, \tag{6}$$

with $\alpha = 1 - 2s$. Here $(X, t) \in \mathbb{R}^n \times \mathbb{R}_+$. Including the boundary conditions the model problem (3) is equivalent to:

$$\begin{aligned} L_s U(x, y, t) &= 0 \quad \text{in } \mathbb{R}^n \times \mathbb{R}_+ \\ U(x, y, 0) &= 0 \quad \text{in } \Omega^C \times \{0\} \\ -\lim_{t \to 0^+} t^\alpha \partial_t U(x, y, t) &= f \quad \text{in } \Omega \times \{0\}. \end{aligned} \tag{7}$$

See Figure 1 for a depiction of the geometry of this boundary value problem when $n = 2$.

After extending f into the upper half space we may equivalently study the interior source problem, with homogeneous boundary conditions:

$$\begin{aligned} L_s U(x, y, t) &= g \quad \text{in } \mathbb{R}^2 \times \mathbb{R}_+ \\ U(x, y, 0) &= 0 \quad \text{in } \Omega^C \times \{0\} \\ -\lim_{t \to 0^+} t^\alpha \partial_t U(x, y, t) &= 0 \quad \text{in } \Omega \times \{0\}. \end{aligned} \tag{8}$$

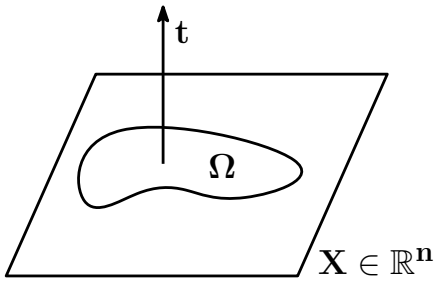

Figure 1: Geometry of the extension problem in the upper half space.

4.1 Boundary (or edge) singularities

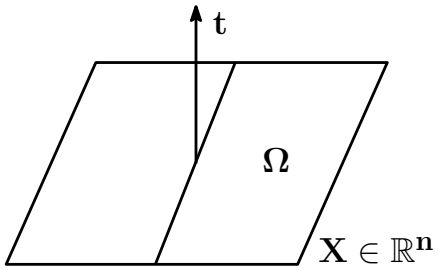

Figure 2: Model geometry for straight boundary.

We first consider the behavior of u near a smooth boundary point of Ω. After straightening out the boundary, the model problem is given by the half space $\Omega = \mathbb{R}_+ \times \mathbb{R}^{n-1}$, depicted in Figure 2.

The problem now becomes one of finding and analyzing a function U in the upper half-space $\mathbb{R}^{n+1}_+$ such that

$$\begin{aligned} L_s U(x, y, t) &= 0 \text{ in } \mathbb{R}^{n+1}_+ \\ U(x, y, 0) &= 0 \text{ for } x < 0,\ y \in \mathbb{R}^{n-1} \\ \lim_{t \to 0^+} t^{1-2s} \partial_t U(x, y, t) &= f \text{ for } x > 0,\ y \in \mathbb{R}^{n-1}. \end{aligned} \tag{9}$$

The translation invariance of this model L_s in y suggests that we conjugate by the Fourier transform in y. Denoting by η the variable dual to y, this gives

$$L_s = \partial_t^2 U + \frac{1-2s}{t}\partial_t U + \partial_x^2 U - |\eta|^2 U \tag{10}$$

and the corresponding boundary problem

$$\begin{aligned} L_s U(x,\eta,t) &= 0 \text{ in } \mathbb{R}^{n+1}_+ \\ U(x,\eta,0) &= 0 \text{ for } x<0, \\ \lim_{t\to 0^+} t^{1-2s}\partial_t U(x,\eta,t) &= f(x,\eta) \text{ for } x>0,\ \eta\in\mathbb{R}^{n-1}. \end{aligned} \tag{11}$$

There is a further reduction if we set $\tau = t|\eta|$ and then divide by $|\eta|^2$. This leads to

$$B(L_s) = \partial_\tau^2 + \frac{1-2s}{\tau}\partial_\tau + \partial_x^2 - 1,$$

which is called the model Bessel operator. The boundary problem is now

$$\begin{aligned} B(L_s) U(x,\eta,\tau/|\eta|) &= 0 \text{ in } \mathbb{R}^{n+1}_+ \\ U(x,\eta,0) &= 0 \text{ for } x<0,\ \eta\in\mathbb{R}^{n-1} \\ \lim_{t\to 0^+} \tau^{1-2s}\partial_\tau U(x,\eta,\tau/|\eta|) &= |\eta|^{2s-3} f(x,\eta) \text{ for } x>0,\ \eta\in\mathbb{R}^{n-1}. \end{aligned} \tag{12}$$

All of the steps above are reversible. In much of the discussion below, we can treat η simply as a parameter. Only at the end, when we take the inverse Fourier transform, is it important to understand this parameter.

Fixing the parameter η, the operator $B(L_s)$ is in the following considered on functions on $\mathbb{R}^2_+$. It is obviously singular at $\tau = 0$, but we are expecting additional singular behavior of solutions at the point $\{x = \tau = 0\}$. To illuminate these, we change the underlying geometry slightly by blowing up the locus $\{x = \tau = 0\}$. In this simple setting, this corresponds to replacing this point with the semicircle of inward-pointing vectors of length one. More concretely, we introduce polar coordinates (ρ,θ)

$$\tau = \rho\sin(\theta),\ x = \rho\cos(\theta)$$

in $\mathbb{R}^2_+$ and then add the 'face' $\rho = 0$ to $\mathbb{R}^2_+ \setminus \{(0,0)\}$. The resulting 'single space', which we denote by $(\mathbb{R}^2_+)_0$, is diffeomorphic to $S^1_+ \times \mathbb{R}^+$.

We now transfer the problem to this space. The lift of the model Bessel operator is

$$B(L_s) = \partial_\rho^2 + \frac{2-2s}{\rho}\partial_\rho + \frac{1}{\rho^2}\left(\partial_\theta^2 + (1-2s)\cot(\theta)\,\partial_\theta\right) - 1. \tag{13}$$

One route toward analyzing $B(L_s)$ is by separation of variables, i.e., by reducing to a family of ordinary differential equations acting on the different eigenspaces of

$$P_s = \partial_\theta^2 + (1-2s)\cot(\theta)\partial_\theta.$$

the operator in θ which appears in parentheses in (13).

P_s with the mixed boundary conditions is nonnegative and self-adjoint on $L^2\left([0,\pi],\sin^{1-2s}(\theta)d\theta\right)$, and by standard arguments, each of these boundary problems has discrete spectrum. We shall use the convention that $P_s\varphi = -\lambda\varphi$ below. These facts are classical in the special case $s = \frac{1}{2}$, i.e., where $P_s = \partial_\theta^2$. Indeed, here the eigenvalues for the mixed problem are $\lambda_j^M = (j+\frac{1}{2})^2$ with eigenfunctions $\varphi_j^M(\theta) = \cos((j+\frac{1}{2})\theta)$.

It is also possible to determine the eigendata for more general values of s explicitly, see [17]:

Lemma 4.1. *The operator P_s is selfadjoint and negative definite on $L^2\left([0,\pi],\sin^{1-2s}(\theta)\,d\theta\right)$ with discrete spectrum. The eigenvalues are $\lambda_j^{M,s} = (j+\frac{1}{2})^2 - (s-\frac{1}{2})^2 = (j+s)(j+1-s)$ with eigenfunctions $\varphi_j^{M,s}(\theta) = \sin^s(\theta)P_j^s(\cos(\theta))$. Here P_ν^s are associated Legendre functions.*

4.2 Corner singularities

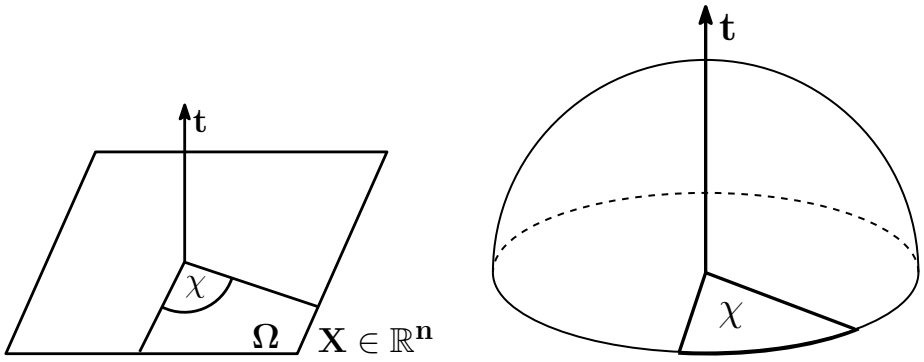

Figure 3: Model geometry for a corner with the opening angle χ.

We now consider the behavior of u near a corner point of Ω. The model problem is then given on $\mathbb{R}^2$ by an infinite sector with opening angle χ. We introduce spherical coordinates around the corner at the origin $(0,0,0)$,

$$t = r\cos(\theta),\ x = r\sin(\theta)\cos(\varphi),\ y = r\sin(\theta)\sin(\varphi).$$

The domain Ω is then defined in spherical coordinates by

$$\Omega = \{(r,\varphi) : r > 0, \varphi \in (0,\chi)\}\ .$$

From the change of coordinates we know that

$$\begin{aligned}
\partial_t U &= \frac{t}{r}\partial_r U + \frac{1}{r}\partial_\theta U, \\
\partial_t^2 U + \Delta_X U &= \frac{1}{r^2}\partial_r(r^2\partial_r U) + \frac{1}{r^2\sin\theta}\partial_\theta(\sin\theta\partial_\theta U) + \frac{1}{r^2\sin^2\theta}\partial_\varphi^2 U \\
&= \partial_r^2 U + \frac{2}{r}\partial_r U + \frac{1}{r^2}\Delta_{\theta,\varphi} U,
\end{aligned}$$

where $\Delta_{\theta,\varphi}$ is the Laplace-Beltrami operator on the 2-sphere S^2, explicitly

$$\Delta_{\theta,\varphi} U = \frac{1}{\sin(\theta)}\partial_\theta(\sin(\theta)\partial_\theta U) + \frac{1}{\sin^2(\theta)}\partial_\varphi^2 U.$$

Ater the change of variables (6) is equivalent to the following expression:

$$L_s U(r,\theta,\varphi) = \partial_r^2 U + \frac{3-2s}{r}\partial_r U + \frac{1}{r^2}(\Delta_{\theta,\varphi} U - (1-2s)\tan(\theta)\partial_\theta U). \tag{14}$$

We define the operator:

$$\mathcal{D}_{\theta,\varphi} U := \Delta_{\theta,\varphi} U - (1-2s)\tan(\theta)\partial_\theta U. \tag{15}$$

Then by taking the Mellin transform of the operator (14) in r, with Mellin transformed variable λ, we obtain the following spectral problem:

$$\begin{aligned}
\mathcal{D}_{\theta,\varphi}\,\hat{\mathrm{u}} &= -\mu^2\,\hat{\mathrm{u}} \quad \text{in } \mathbb{S}^2 \cap \mathbb{R}^3_+ = S^2_+ \\
\lim_{\theta\to\frac{\pi}{2}} \left(\frac{\pi}{2} - \theta\right)^\alpha \partial_\theta\,\hat{\mathrm{u}} &= 0, \quad \text{for } \varphi \in (0,\chi), \\
\hat{\mathrm{u}} &= 0 \quad \text{for } \varphi \notin (0,\chi),\ \theta = \pi/2.
\end{aligned} \tag{16}$$

Here we have set $\mu^2 = \lambda^2 + (2-2s)\lambda$.

Lemma 4.2. *The operator $\mathcal{D}_{\theta,\varphi}$ with the mixed boundary conditions in* (16) *is selfadjoint and negative in $H = L^2(S^2_+, \cos^{1-2s}(\theta) dS)$ with discrete spectrum. The eigenvalues $-\mu^2$ of $\mathcal{D}_{\theta,\varphi}$ determine the corner exponents λ of the solution u via $\mu^2 = \lambda^2 + (2-2s)\lambda$.*

For $s = \frac{1}{2}$ we recover the classical analysis of the Laplace equation with mixed boundary conditions, while for $s \neq \frac{1}{2}$ the spectral problem involves the operator $\mathcal{D}_{\theta,\varphi}$ instead of the Laplace-Beltrami operator.

Note that (16) cannot be simplified further by separation of the coordinates θ and φ, because of the φ-dependent boundary condition on the equator.

The proof of the lemma follows from an analysis of the bilinear form on H associated to $\mathcal{D}_{\theta,\varphi}$:

$$\mathsf{b}(u,v) = -\langle \mathcal{D}_{\theta,\varphi} u, v\rangle_H = \int_{S^2_+} \sin(\theta)\cos^{1-2s}(\theta)(\partial_\theta u)(\partial_\theta v) + \sin(\theta)^{-1}\cos^{1-2s}(\theta)(\partial_\varphi u)(\partial_\varphi v)\ . \tag{17}$$

In particular, the domain of the closure of b compactly embeds in H, so that $\mathcal{D}_{\theta,\varphi}$ has discrete spectrum. The smallest eigenvalue μ_0^2 is given by

$$\mu_0^2 = \min_{\|v\|_H=1} \mathsf{b}(v,v) > 0\ . \tag{18}$$

Corollary 4.3. *μ_0^2 is a decreasing function of $\chi \in (0, 2\pi)$. μ_0^2 is a increasing function of $s \in (0,1)$ with $\partial_s \mu_0^2 > 2$.*

Proof. The first assertion follows from domain monotonicity: The set Ω^C on which Dirichlet conditions are imposed on v shrinks with χ, so that the minimum in (18) is an increasing set of functions.

For the second assertion we use standard perturbation theory of eigenvalues for a holomorphic family of operators [24, p. 405]. However, this theory has been developed for families of operators on a fixed Hilbert space, while here $H = L^2(S^2_+, \cos^{1-2s}(\theta) dS)$ depends on s through the weighted Lebesgue measure $w(\theta) d\theta d\varphi = \cos^{1-2s}(\theta)\sin(\theta) d\theta d\varphi$.

Instead of $\mathcal{D}_{\theta,\varphi}$, we therefore consider the operator $\widetilde{\mathcal{D}}_{\theta,\varphi} = T \circ \mathcal{D}_{\theta,\varphi} \circ T^{-1}$, which acts on the s-independent Hilbert space $T(H) = L^2(S^2_+, d\theta d\varphi)$, where $Tv = vw^{1/2}$. $\widetilde{\mathcal{D}}_{\theta,\varphi}$ has the same spectrum as $\mathcal{D}_{\theta,\varphi}$.
Since

$$\begin{aligned} w(\theta)^{1/2}\partial_\theta(w(\theta)^{-1/2}) &= -\frac{1}{2}\left(\cot(\theta) - \alpha\tan(\theta)\right), \\ w(\theta)^{1/2}\partial_\theta^2(w(\theta)^{-1/2}) &= \frac{3}{4}\cot^2(\theta) + \left(s^2 - 2s + \frac{3}{4}\right)\tan^2(\theta) - (2s^2 - 4s + 1). \end{aligned}$$

$\widetilde{\mathcal{D}}_{\theta,\varphi}$ is then explicitly given by

$$\begin{aligned} \widetilde{\mathcal{D}}_{\theta,\varphi} V &= \partial_\theta^2 V + \frac{1}{\sin^2(\theta)}\partial_\varphi^2 V + \left(\cot(\theta) - \alpha\tan(\theta) + 2w(\theta)^{1/2}\partial_\theta(w(\theta)^{-1/2})\right)\partial_\theta V \\ &\quad + \left(\left(\cot(\theta) - \alpha\tan(\theta)\right) w(\theta)^{1/2}\partial_\theta(w(\theta)^{-1/2}) + w(\theta)^{1/2}\partial_\theta^2(w(\theta)^{-1/2})\right) V \\ &= \partial_\theta^2 V + \tfrac{1}{\sin^2(\theta)}\partial_\varphi^2 V + \tfrac{1}{4}\cot^2(\theta) V + \left[(\alpha + \tfrac{1}{2}) + \tfrac{\alpha}{2}(1 - \tfrac{\alpha}{2})\tan^2(\theta)\right] V, \end{aligned}$$

where $\alpha = 1 - 2s$ as above. If $\Phi_{0,s}$ denotes the eigenfunction associated to the eigenvalue $-\mu_0^2$ for a given $s \in (0,1)$, the derivative of $-\mu_0^2$ with respect to s is given according to perturbation theory by

$$-\partial_s \mu_0^2 = \langle \Phi_{0,s}, (\partial_s \widetilde{\mathcal{D}}_{\theta,\varphi})\Phi_{0,s}\rangle_{L^2(S^2_+, d\theta d\varphi)} = \langle \Phi_{0,s}, -2(1 + s\tan(\theta)^2)\Phi_{0,s}\rangle_{L^2(S^2_+, d\theta d\varphi)} < -2.$$

This proves the second part, μ_0^2 is an increasing function of $s \in (0,1)$ with $\partial_s \mu_0^2 > 2$.

□

Corollary 4.4. *λ_0 is a decreasing function of $\chi \in (0, 2\pi)$. λ_0 is a increasing function of $s \in (0,1)$ with $\lambda_0 > \max(0, s - \frac{1}{2})$.*

Proof. As μ^2 and λ are connected by a monotonous relation, $\mu^2 = \lambda^2 + (2-2s)\lambda$ and $\mu_0^2 > 0$ it follows that $\lambda > 0$. We further define a function $f(s) = 2s - s^2 - 3/4$. Note that $\lambda(s) > s - \frac{1}{2}$ when $\mu^2 > f(s)$. By Corollary 4.3 $\partial_s \mu_0^2(s) > 2 > 2 - 2s = \partial_s f(s)$ for all $s \in (0,1)$. Furthermore, since $\mu_0^2(0) = 0 > -3/4 = f(0)$, it follows that $\mu_0^2(s) > f(s)$ for all $s \in (0,1)$. Therefore, $\lambda(s) > \max(0, s - \frac{1}{2})$. □

Remark 4.5. For $s = 1$, we note that $\lambda = \frac{\pi}{\chi}$.

4.3 Edge-corner singularities

The eigenfunctions $\hat{u}_j$ of (16) are not smooth, but exhibit singularities as $\theta \to \frac{\pi}{2}$, because of the mixed boundary conditions and the singular behavior of the first-order term $(1-2s)\tan(\theta)\partial_\theta$ in the operator $\mathcal{D}_{\theta,\varphi}$.

We first discuss the local behavior near $(\theta, \varphi) = (\frac{\pi}{2}, 0)$, where the boundary conditions jump. The discussion equally applies to the local behavior near $(\theta, \varphi) = (\frac{\pi}{2}, \chi)$. For $\varphi \notin \{0, \chi\}$, the trace of $\hat{u}_j$ on the equator $\theta = \frac{\pi}{2}$ is smooth, and the corresponding singularities of the solution U to the extended problem are not relevant to the solution u of the fractional boundary problem.

To understand the behavior around $(\theta, \varphi) = (\frac{\pi}{2}, 0)$, we introduce polar coordinates (ϱ, ω),

$$\frac{\pi}{2} - \theta = \varrho \sin(\omega), \;\; \varphi = \varrho \cos(\omega) \; .$$

The Laplace-Beltrami operator $\Delta_{\theta,\varphi}$ then becomes

$$\begin{aligned} \Delta_{\theta,\varphi} &= \frac{1}{\sin(\theta)} \partial_\theta (\sin(\theta) \partial_\theta) + \frac{1}{\sin^2(\theta)} \partial_\varphi^2 \\ &= \partial_\theta^2 + \partial_\varphi^2 + R_1 = \partial_\varrho^2 + \frac{1}{\varrho} \partial_\varrho + \frac{1}{\varrho^2} \partial_\omega^2 + R_1, \end{aligned}$$

where

$$R_1 = (\cot(\theta) - 1)\partial_\theta + \left(\frac{1}{\sin^2(\theta)} - 1 \right) \partial_\theta^2$$

is of lower order at $\theta = \frac{\pi}{2}$ and does not affect the singular behavior.

The second term, $(1-2s)\tan(\theta)\partial_\theta$, in the operator $\mathcal{D}_{\theta,\varphi}$ is analogous to the edge case (13):

$$\begin{aligned} \tan(\theta)\partial_\theta &= \frac{1}{\frac{\pi}{2} - \theta} \partial_\theta + R_2 \\ &= \frac{1}{\varrho \sin(\omega)} \left(\sin(\omega) \partial_\varrho + \frac{1}{\rho} \cos(\omega) \partial_\omega \right) + R_2 \\ &= \frac{1}{\varrho} \partial_\varrho + \frac{1}{\varrho^2} \cot(\omega) \partial_\omega + R_2 \; , \end{aligned}$$

where $R_2 = (\tan(\theta) - \frac{1}{\frac{\pi}{2} - \theta})\partial_\theta$ does not affect the singularities. We conclude that up to the negligible terms R_1, R_2,

$$\begin{aligned} \mathcal{D}_{\theta,\varphi} &= \partial_\varrho^2 + \frac{2-2s}{\varrho} \partial_\varrho + \frac{1}{\varrho^2} \left(\partial_\omega^2 + (1-2s)\cot(\omega)\partial_\omega \right) \\ &= \partial_\varrho^2 + \frac{2-2s}{\varrho} \partial_\varrho + \frac{1}{\varrho^2} P_\omega \; . \end{aligned}$$

Up to lower order terms, near $\varrho = 0$ we therefore recover an operator as in (13), whose spectral data are given by Lemma 4.1. We conclude that near $\varrho = 0$ the eigenfunctions $\hat{u}_j$ of $\mathcal{D}_{\theta,\varphi}$ admit an expansion

$$\hat{u}_j \sim \sum_k \hat{u}_{j,k} \varrho^{s+k} P_k^s(\cos(\omega)) \sin^s(\omega) \ .$$

5 Asymptotic expansions and approximation properties

In this section we summarize the conclusions from the previous section: The solution to the fractional Laplace equation with Dirichlet boundary conditions near the boundary or a corner admits a decomposition into the edge, corner and edge-corner singularities, plus a regular remainder. Such a decomposition allows us to derive optimal convergence rates on graded meshes.

More precisely, from Section 4 the solution to the extended problem (3) near the vertex of $\Omega = \{(r, \varphi) : r > 0, \varphi \in (0, \chi)\}$ admits an expansion of the form

$$U(r, \theta, \varphi) \sim \sum_j \sum_{k=0}^{N_j} r^{\lambda_j} \log(r)^k \hat{u}_{jk}(\theta, \varphi),$$

up to a smooth remainder, where $\hat{u}_{jk}$ are the eigenfunctions corresponding to a spectral problem on S^2_+ with mixed boundary conditions. Here $\lambda_j > \max\{s - \frac{1}{2}, 0\}$.

The solution to the original fractional problem (3) is given by the trace at $\theta = \frac{\pi}{2}$, $u(r, \varphi) = U(r, \frac{\pi}{2}, \varphi)$. When φ is strictly between 0 and χ, the trace of the eigenfunction $\hat{u}_j(\frac{\pi}{2}, \varphi)$ is smooth and the asymptotic expansion takes the form

$$u(r, \varphi) \sim \sum_j \sum_{k=0}^{N_j} r^{\lambda_j} \log(r)^k \hat{u}_{jk}(\tfrac{\pi}{2}, \varphi) \tag{19}$$

with smooth coefficient functions.

Translating from (r, φ) back to (x, y), $r = \sqrt{x^2 + y^2}$, while $\varphi = \tan^{-1}(y/x)$ is a smooth function of x and y in this region. Therefore

$$u(x, y) \sim \sum_j \sum_{k=0}^{N_j} \hat{U}_{jk}(x, y) \ (x^2 + y^2)^{\lambda_j/2} \log(x^2 + y^2)^k \tag{20}$$

$$. \tag{21}$$

The behavior at the boundaries $\varphi = 0$ and $\varphi = \chi$ is analogous, and we only discuss the edge-vertex singularities for $\varphi = 0$. There $\hat{u}_{jk} \sim \sum_l \sum_{m=1}^{M_l} \hat{u}_{jk,lm} \varrho^{s+l} \log(\varrho)^m P_l^s(\cos(\omega)) \sin^s(\omega)$. The trace u at $\theta = \frac{\pi}{2}$ corresponds to $\varrho \sim \varphi$ and $\omega = 0$, so that

$$\hat{u}_{jk}(\tfrac{\pi}{2}, \varphi) \sim \textstyle\sum_l \sum_{m=1}^{M_l} \hat{u}_{jk,lm} \varphi^{s+l} \log(\varphi)^m$$

near $\varphi = 0$. Therefore in this region

$$u(r, \varphi) \sim \sum_{j,k,l,m} \widetilde{u}_{jk,lm} r^{\lambda_j} \log(r)^k \varphi^{s+l} \log(\varphi)^m \ . \tag{22}$$

Translating from (r, φ) back to (x, y), we expand sine and cosine into a Taylor series at $\varphi = 0$ to see

$$y \sim r\varphi + r \sum_{i>2} a_i \varphi^i, \quad x \sim r + r \sum_{i>1} a_i \varphi^i \ ,$$

or up to higher order terms

$$r \sim x, \quad \varphi \sim y/x \ .$$

We conclude that in Cartesian coordinates near $\varphi = 0$, i.e. $y = 0$, u has an expansion of the form

$$u(x,y) \sim \sum_{j,k,l,m} \widehat{u}_{jk,lm} x^{\lambda_j - s - l} y^{s+l} \log(x)^k \log(y)^m \ . \tag{23}$$

We summarize this discussion in the following theorem:

Theorem 5.1. *Let $u \in \widetilde{H}^s(\Omega)$ be the solution to (3) for $f \in C^\infty(\overline{\Omega})$ in a polygonal domain $\Omega \subset \mathbb{R}^2$. Then in polar coordinates in a neighborhood of each vertex of Ω*

$$u(r,\varphi) \sim u_0 + \sum_{j,k,l,m} \widetilde{u}_{jk,lm} r^{\lambda_j} \log(r)^k \varphi^{s+l} \log(\varphi)^m \ , \tag{24}$$

where u_0 is sufficiently smooth. In Cartesian coordinates, this corresponds to a vertex singularity

$$u(x,y) \sim \sum_j \sum_{k=0}^{N_j} \hat{U}_{jk}(x,y) \ (x^2+y^2)^{\lambda_j/2} \log(x^2+y^2)^k \tag{25}$$

away from the edge $\varphi = 0$, i.e. $y = 0$.
The edge-vertex singularity near $\varphi = 0$, i.e. $y = 0$, is of the form

$$u(x,y) \sim \sum_{j,k,l,m} \widehat{u}_{jk,lm} x^{\lambda_j - s - l} y^{s+l} \log(x)^k \log(y)^m \tag{26}$$

Away from the vertex, in a neighborhood of the edge at $\varphi = 0$, i.e. $y = 0$,

$$u(x,y) \sim \sum_{j,k} \bar{u}_{jk}(x) y^{s+j} \log(y)^k \ . \tag{27}$$

The logarithms in the expansion only occur for integer singular exponents or for singular exponents corresponding to multiple eigenvalues. For simplicity, we focus on the approximation of the singular functions without logarithmic terms.

For the numerical approximation, without loss of generality we assume that Ω has a polygonal boundary. Let $\mathcal{T}_h$ be a family of shape-regular triangulations of Ω and $\mathbb{V}_h \subset \widetilde{H}^s(\Omega)$, the associated space of continuous piecewise linear functions on $\mathcal{T}_h$, vanishing at the boundary.

The discretized problem is given by:

Find $u_h \in \mathbb{V}_h$, such that for all $v \in \mathbb{V}_h$

$$\mathsf{a}(u,v) = (f,v)_{L^2(\Omega)} \ .$$

By coercivity, there exists a unique solution.

This discretized problem is solved on either quasi-uniform or on graded triangulations $\mathcal{T}_h$ of Ω. To define a β-graded mesh on a square or a disc, it suffices to consider β-graded meshes on the unit interval $[-1,0]$. For the square, we consider $x_k = y_k = -1 + (\frac{k}{N})^\beta$ for $k = 1,\dots,N$ and the grading parameter $\beta \geq 1$. The nodes of the β-graded mesh on a square are then given by (x_k, y_ℓ), for $k,\ell = 1,\dots,N$. Note that for $\beta = 1$ we obtain an uniform mesh.
On a disc, to obtain a β-graded mesh, the radii r_k are shifted towards the boundary. In particular, on the unit disk the radii are given by $r_k = \left(1 - (\frac{k}{N})^\beta\right)$, with the total number of triangles proportional to N^2.
Examples of 2-graded meshes are depicted in Figure 4.

For the construction of graded meshes on a polygonal domain Ω, we first consider the case of a triangle. On a general polygon Ω the construction is similar, or one can first subdivide the

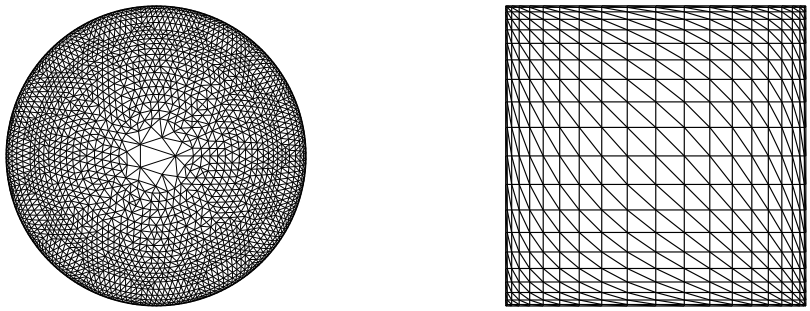

Figure 4: β-graded meshes with $\beta = 2$ for the unit disc and the unit square.

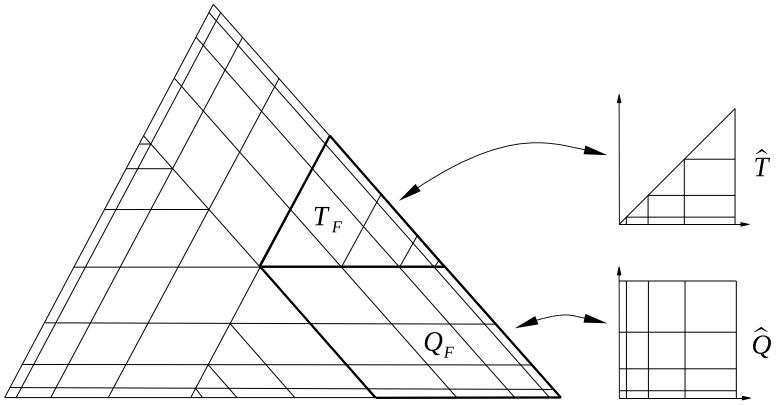

Figure 5: Graded mesh on the triangle $F \subset \Omega$. The triangular (resp. parallelogram) block of elements T_F (resp. Q_F) is the image of the graded mesh on the unit triangle $\hat{T}$ (resp. the unit square $\hat{Q}$).

polygon into triangles. On a triangle, we first draw three lines through the centroid and parallel to the sides of Ω. This divides Ω into three parallelograms and three triangles as in Figure 5. Each of the three parallelograms can be mapped onto the unit square $\hat{Q} = (0,1)^2$ by a linear transformation such that the vertex $(0,0)$ of $\hat{Q}$ is the image of a vertex of Ω. Analogously, each of the three sub-triangles can be mapped onto the unit triangle $\hat{T} = \{(x_1, x_2); 0 < x_1 < 1, 0 < x_2 < x_1\} \subset \hat{Q}$ such that the vertex $(1,1)$ of $\hat{T}$ is the image of the centroid of Ω. Then the β-graded mesh on $\hat{Q}$ (and therefore on $\hat{T}$) is generated by the lines

$$x_1 = \left(\frac{i}{N}\right)^\beta \qquad x_2 = \left(\frac{j}{N}\right)^\beta \quad i, j = 0, 1, \ldots, N,$$

for given refinement level N. Mapping each cell of these meshes back onto Ω, we obtain a β-graded mesh of triangles and parallelograms on F as in Figure 5. The diameter of the largest element of this mesh is proportional to βN^{-1}.

The following approximation results will be shown below.

Theorem 5.2. *Let $u \in \widetilde{H}^s(\Omega)$ be a solution to (1) and $\Pi_h u$ be the best approximation by p.w. linear functions on a β-graded mesh in the $\widetilde{H}^s(\Omega)$ norm.*
Then for $\beta > \frac{2-s}{\nu(s)+\frac{1}{2}-s}$

$$\|u - \Pi_h u\|_{\widetilde{H}^s(\Omega)} \leq C_{\beta,\varepsilon} h^{\min\{\beta\nu(s), 2-s\}-\varepsilon}.$$

Corollary 5.3. *Let $u \in \widetilde{H}^s(\Omega)$ be a solution to (1) and $u_h \in \widetilde{H}^s(\Omega)$ be the finite element approximation by p.w. linear functions on β-graded meshes.*
Then for $\beta > \frac{2-s}{\nu(s)+\frac{1}{2}-s}$

$$\|u - u_h\|_{\widetilde{H}^s(\Omega)} \leq C_{\beta,\varepsilon} h^{\min\{\beta\nu(s),2-s\}-\varepsilon}.$$

This generalizes approximation results [2, Theorem 4.11] for convex domains.

6 Approximation results in polygons

This section provides the proof of Theorem 5.2.

We first recall the following 1d approximation result from Satz 3.10 [30]:

Theorem 6.1. *For $a > 0$ and $s \in [0, a+\frac{1}{2})$ there holds with the linear interpolant $\Pi_y^1 y^a$ of y^a*

$$\|y^a - \Pi_y^1 y^a\|_{\widetilde{H}^s([0,1])} \lesssim h^{\min\{\beta(a-s+\frac{1}{2})-\varepsilon,2-s\}} ,$$

provided $\beta > \frac{2-s}{a+\frac{1}{2}-s}$.

To discuss the approximation properties of graded meshes, we introduce anisotropic Sobolev spaces.

Definition 6.2. Let Q be a Lipschitz domain. $H^{(1,0)}(Q)$ denotes the closure of $C^\infty(Q)$ in the norm

$$\|u\|^2_{H^{(1,0)}(Q)} := \|u\|^2_{L^2(Q)} + \|u_x\|^2_{L^2(Q)}.$$

We define the anisotropic space $H^{(\sigma,0)}(Q)$ by interpolation:

$$H^{(\sigma,0)}(Q) := \Big(L^2(Q), H^{(1,0)}(Q)\Big)_{[\sigma]}, \quad H^{(0,\sigma)}(Q) := \Big(L^2(Q), H^{(0,1)}(Q)\Big)_{[\sigma]}$$

Note that for the homogeneous Sobolev spaces we have for $\sigma \geqslant 0$

$$H^\sigma(Q) = H^{(\sigma,0)}(Q) \cap H^{(0,\sigma)}(Q)$$

and

$$\|u\|_{H^\sigma(Q)} \leqslant C\|u\|_{H^{(\sigma,0)}(Q)} + C\|u\|_{H^{(0,\sigma)}(Q)}.$$

Further we shall need Sobolev spaces with a Dirichlet boundary condition imposed on a part of the boundary.

Definition 6.3. Let Q be a Lipschitz domain, $\Gamma_0 \cap \overline{Q} \subset \partial Q$ part of the boundary, $0 \leqslant \sigma \leqslant 1$.

$$\overset{\circ}{H}{}^1_{\Gamma_0}(Q) := \big\{u \in H^1(Q) |\ u|_{\Gamma_0} = 0\big\}$$
$$\tilde{H}^\sigma_{\Gamma_0}(Q) := \Big(L^2(Q), \overset{\circ}{H}{}^1_{\Gamma_0}(Q)\Big)_{[\sigma]}$$

For $\sigma \neq 1/2$ we can estimate the norm of a function by the norms in the subdomains, but with constants depending on the domains.

Lemma 6.4. *Let Q, Q_1, Q_2 be Lipschitz with $\overline{Q} = \overline{Q_1} \bigcup \overline{Q_2}, \overline{Q_0} = \partial Q_1 \cap \partial Q_2, \partial Q_1 = \overline{\Gamma_0} \bigcup \overline{\Gamma_1}, \partial Q_2 = \overline{\Gamma_0} \bigcup \overline{\Gamma_2}, 0 \leqslant \sigma \leqslant 1, \sigma \neq \frac{1}{2}$. Then there exists a constant $c > 0$ such that for all $u \in H^\sigma(Q), \tilde{u} \in \tilde{H}^\sigma(Q)$ there holds*

$$\|u\|_{H^\sigma(Q)} \leqslant c\|u\|_{H^\sigma(Q_1)} + c\|u\|_{H^\sigma(Q_2)}$$
$$\|\tilde{u}\|_{\tilde{H}^\sigma(Q)} \leqslant c\|u\|_{\tilde{H}^\sigma_{\Gamma_1}(Q_1)} + c\|u\|_{\tilde{H}^\sigma_{\Gamma_2}(Q_2)} .$$

Similary, there exists a constant $c > 0$ such that for all $u \in H^(0,\sigma)(Q)$ there holds

$$\|u\|_{H^{(0,\sigma)}(Q)} \leqslant c\|u\|_{H^{(0,\sigma)}(Q_1)} + c\|u\|_{H^{(0,\sigma)}(Q_2)} .$$

Proof. Consider the mapping T which maps $u \in H^\sigma(Q)$ into $(u|_{Q_1}, u|_{Q_2}) \in H^\sigma(Q_1) \times H^\sigma(Q_2)$. For $\sigma \neq \frac{1}{2}$ the range of T is closed in $H^\sigma(Q_1) \times H^\sigma(Q_2)$ which is equivalent to $\mathring{H}^\sigma(Q) = \tilde{H}^\sigma(Q)$ for $\sigma \neq \frac{1}{2}$. Hence the assertion of the lemma follows from the closed graph theorem. The proof for $H^{(0,\sigma)}(Q)$ is analogous. □

We now consider the approximation by bilinear functions on a rectangle.

Lemma 6.5 (Lemma 7.7, [23], Lemma 3.14, [30]). *Let $Q = [0, h_1] \times [0, h_2], u \in H^3(Q), p$ the bilinear interpolant of u at the vertices of Q. Then there holds*

$$\|u - p\|_{L^2(Q)} \leqslant C \left(h_1^2 \|u_{xx}\|_{L^2(Q)} + h_2^2 \|u_{yy}\|_{L^2(Q)} + h_1^2 h_2 \|u_{xxy}\|_{L^2(Q)} \right) , \tag{28}$$

$$\|(u - p)_x\|_{L^2(Q)} \leqslant C \left(h_1 \|u_{xx}\|_{L^2(Q)} + h_2^2 \|u_{xyy}\|_{L^2(Q)} \right) , \tag{29}$$

$$\|(u - p)_y\|_{L^2(Q)} \leqslant C \left(h_2 \|u_{yy}\|_{L^2(Q)} + h_1^2 \|u_{xxy}\|_{L^2(Q)} \right) . \tag{30}$$

We can now begin the proof of the approximation theorem, Theorem 5.2. After a linear change of coordinates we may assume that we consider a function u on a rectangular domain, see p. 247 in [31]. The decomposition in Theorem 5.1 then becomes

$$\begin{aligned} u(x, y) = \hat{\chi}(r) r^\gamma \alpha(\varphi) + \tilde{\chi}(x) B_1(x, y) x^{\lambda - s} y^s \\ + \tilde{\chi}(y) B_2(x, y) y^{\lambda - s} x^s + u_0(r, \varphi) , \end{aligned} \tag{31}$$

and we discuss the approximation of the individual terms below. While we use triangular meshes in our computations, for the ease of presentation we firstdiscuss the approximation properties of graded meshes with rectangular elements. Reference [30] shows how to deduce approximation results on triangular meshes from the rectangular case.

6.1 Approximation of regular part

Let $p \in S_h^\beta$ denote the interpolant of v^0, where S_h^β are the piecewise linear functions on the graded mesh $x_j = (jh)^\beta$, $y_k = (kh)^\beta$. Hence with $R_{jk} = (x_{j-1}, x_j) \times (y_{k-1}, y_k)$

$$\begin{aligned} \|v^0 - p\|^2_{L^2(Q)} = \sum_{j,k=1}^N \|v^0 - p\|^2_{L^2(R_{jk})} \leqslant \sum_{j,k=1}^N \Big(h_j^4 \|v^0_{xx}\|^2_{L^2(R_{jk})} + h_k^4 \|v^0_{yy}\|^2_{L^2(R_{jk})} \\ + h_j^4 h_k^2 \|v^0_{xxy}\|^2_{L^2(R_{jk})} \Big) \lesssim h^4 \|v^0\|^2_{H^3(Q)} \end{aligned}$$

$$\begin{aligned} \|v^0 - p\|^2_{H^1(R_{jk})} = \sum_{j,k=1}^N \|v^0 - p\|^2_{H^1(R_{jk})} \leqslant \sum_{j,k=1}^N c \Big(h_j^2 \|v^0_{xx}\|^2_{L^2(R_{jk})} + h_k^2 \|v^0_{yy}\|^2_{L^2(R_{jk})} \\ + h_j^4 \|v^0_{xxy}\|^2_{L^2(R_{jk})} + h_k^4 \|v^0_{xyy}\|^2_{L^2(R_{jk})} \Big) \lesssim h^2 \|v^0\|^2_{H^3(Q)} \end{aligned}$$

Interpolation yields $\|v^0 - p\|_{H^s(Q)} \lesssim h^{2-s} \|v^0\|_{H^3(Q)}$.

6.2 Approximation of corner singularity

$u = r^\lambda \alpha(\varphi)$ with $w \in H^3([0, \pi/2])$. We devide the square $Q = [0, 1]^2$ in $N - 1$ overlapping domains $A_j, j = 1, \ldots, N - 1$.

$$A_j = \bigcup \{ R_{kl} | j \leqslant k \leqslant j + 1, l \leqslant k \text{ or } j \leqslant l \leqslant j + 1, k \leqslant l \}$$

Further we take a partition of unity $\{\chi_j\}$ on Q w.r.t. the sets A_j, e.g. let χ_{kl} the piecewise bilinear function on the mesh, which is 1 at (x_k, x_l) and 0 at all other nodes. We take $\chi_j = \sum \{\chi_{kl} | \text{supp} \chi_{kl} \subset A_j\}$. Then $|(\chi_j)_x| \leqslant h_j^{-1}, |(\chi_j)_y| \leqslant h_j^{-1}$.

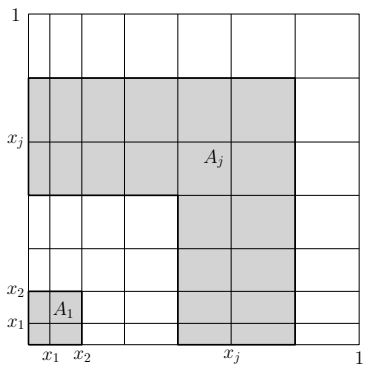

Figure 6: The domains A_j.

We estimate the approximation error in each A_j in L^2 and H^1; then interpolation gives an upper bound for $\chi_j(u-p)$ in $\tilde{H}^s$. This is then used to derive the estimate on Q.
For $j > 1$ with $h_k \le h_{j+1}$ when $R_{kl} \subset A_j$ we have

$$\|u-p\|^2_{L^2(A_j)} \leqslant \sum_{R_{kl}} c\left(h_k^4\|u_{xx}\|^2_{L^2(R_{kl})} + h_l^4\|u_{yy}\|^2_{L^2(R_{kl})} + h_k^4 h_l^2\|u_{xxy}\|^2_{L^2(R_{kl})}\right)$$

$$\begin{aligned}\|u-p\|^2_{H^1(A_j)} \leqslant c\Big(&h_{j+1}^2\|u_{xx}\|_{L^2(A_j)} + h_{j+1}^2\|u_{yy}\|_{L^2(A_j)} \\ &+ h_{j+1}^4\|u_{xxy}\|^2_{L^2(A_j)} + h_{j+1}^4\|u_{xyy}\|^2_{L^2(A_j)}\Big)\end{aligned}$$

This implies with $u = r^\lambda\alpha(\varphi)$

$$\|u-p\|^2_{L^2(A_j)} \leqslant (C\,h_{j+1}x_{j-1})\left(h_{j+1}^4 x_{j-1}^{2\lambda-4} + h_{j+1}^6 x_{j-1}^{2\lambda-6}\right)$$
$$\|u-p\|^2_{H^1(A_j)} \leqslant (C\,h_{j+1}x_{j+1})\left(h_{j+1}^2 x_{j-1}^{2\lambda-4} + h_{j+1}^4 x_{j-1}^{2\lambda-6}\right)$$

Note that χ_j vanishes on $\zeta_j := \partial A_j \setminus \partial Q$, hence interpolation yields

$$\|\chi_j(u-p)\|^2_{\tilde{H}^s_{\zeta_j}(A_j)} \leqslant (C\,h_{j+1}x_{j+1})\left(h_{j+1}^{4-2s}x_{j-1}^{2\lambda-4}\right).$$

Since $r^\lambda \in H^1(Q)$ we have for $j = 1$

$$\|u-p\|^2_{L^2(A_1)} \leqslant C x_2^{2\lambda+2}, \qquad \|u-p\|^2_{H^1(A_1)} \leqslant C\,x_2^{2\lambda},$$

hence

$$\|\chi_1(u-p)\|^2_{\tilde{H}^s_{\zeta_1}(A_1)} \leqslant C\,x_2^{2\lambda+2-2s}$$

Since the terms $\chi_j(u-p)$ with even and odd j have disjoint supports and vanish on ζ_j, there holds

$$\|u-p\|^2_{H^s(Q)} \leqslant 2\sum_{j\ \text{odd}} \|\chi_j(u-p)\|^2_{\tilde{H}^s_{\zeta_j}(A_j)} + 2\sum_{j\ \text{even}} \|\chi_j(u-p)\|^2_{\tilde{H}^s_{\zeta_j}(A_j)}$$

Due to $h_k \leqslant \beta x_k^\gamma h$ with $\gamma := 1 - 1/\beta$ the terms for $j = 2, \dots, N-1$ are bounded by

$$C\sum_{j=2}^{N-1} h_{j+1}^{5-2s}x_{j+1}^{2\lambda-3} \leqslant C\,h^{4-2s}\int_{x_2}^{1} x^{2\lambda-3+(4-2s)\gamma}dx = \mathcal{O}(h^{4-2s}) \quad \text{for } \beta > \frac{2-s}{\lambda+1-s}.$$

Also the term with $j = 1$ is of same order. Hence in total for the corner singularity we have convergence rate h^{2-s} in $H^s(Q)$.

6.3 Approximation of singular edge functions

We next consider the approximation of the singular edge functions

$$f(x,y) = x^{\lambda-\nu} y^{\nu} \tilde{\chi}(x) \tag{32}$$

with corner exponent λ, edge exponent ν and cut-off function χ with $\chi(\theta) = 1$ near $\theta = 0$. Divide $Q = (0,1)^2$ into 2 triangles

$$A_: = \{(x,y) \in Q | y \leqslant x\}, \quad B := \{(x,y) \in Q | y > x\},$$

and estimate the interpolation error on each triangle in $H^{s+\varepsilon}$, $0 \leq \epsilon \leq 1-s$. Lemma 6.4 yields error bound in $H^{s+\varepsilon}(Q)$.
On triangle B there holds $f(x,y) = r^{\lambda} w(\theta)$ with $w(\theta)$ smooth on $[\frac{\pi}{4}, \frac{\pi}{2}]$. Extend $w(\theta)$ to a smooth function $\tilde{w}(\theta)$ on $[0, \frac{\pi}{2}]$ and define $\tilde{f}(x,y) := r^{\lambda}\tilde{w}(\theta)$. Now $\tilde{f}$ can be approximated on Q like a corner singularity and for its interpolant $\tilde{p}$ there holds

$$\|\tilde{f} - \tilde{p}\|_{H^{s+\varepsilon}(Q)} \leqslant c\, h^{2-s-\varepsilon}$$

yielding, by restriction to B,

$$\|f - p\|_{H^{s+\varepsilon}(B)} \leqslant c\, h^{2-s-\varepsilon}.$$

On triangle A we estimate the approximation error separately in the anisotropic spaces $H^{(\sigma,0)}$ and $H^{(0,\sigma)}$ with $\sigma > 1/2$. Consider the larger domain $\tilde{A}$ with (see Figure 7)

$$A \subset \tilde{A} := \bigcup \{R_{kl} | l \leqslant k+1\}$$

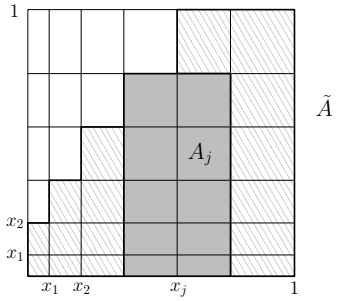

Figure 7: The rectangles A_j

Let $\chi_j(x)$ be piecewise linear on $0 < x_1 < \cdots < x_{N-1} < 1$ with $\chi_j(x_j) = 1$ and vanishing in the other nodes, $j = 2, \ldots, N-2$. χ_1 pw. linear with $\chi_1(0) = \chi_1(x_1) = 1$ and $\chi_1(x_j) = 0$ for $j > 1$. χ_{N-1} pw. linear with $\chi_{N-1}(x_{N-1}) = \chi_{N-1}(1) = 1$ and $\chi_{N-1}(x_j) = 0$ for $j < N-1$. Divide $\tilde{A}$ into overlapping rectangles $A_j = [x_{j-1}, x_{j+1}] \times [0, x_{j+1}]$, $j = 1, \ldots, N-1$. With

$$g_j := \begin{cases} (f(x,y) - p(x,y))\, \chi_j(x) \text{ on } A_j \\ 0 \text{ else} \end{cases} \tag{33}$$

there holds $f - p = \sum_{j=1}^{N-1} g_j$. With $\chi(\theta) \equiv 1$ on $A_2, ..., A_{N-1}$ in (32) we have $f(x,y) = f_1(x) f_2(y)$ with $f_1(x) := x^{\lambda-\nu}$, $f_2(y) := y^{\nu}$. Let ζ_j denote the *left and right* boundary of A_j for $j = 2, \ldots, N-2$; ζ_1 the *right boundary* of A_1, ζ_{N-1} the *left boundary* of A_{N-1}. Then

$$\|\sum_{j=1}^{N-1} g_j\|^2_{H^{(\sigma,0)}(\tilde{A})} \leqslant 2 \sum_{j \text{ odd}} \|g_j\|_{\tilde{H}^{(\sigma,0)}_{\zeta_j}(A_j)} + 2 \sum_{j \text{ even}} \|g_j\|_{\tilde{H}^{(\sigma,0)}_{\zeta_j}(A_j)}$$

Now for $j \geqslant 2$ we have with the interpolant p_j of f_j:

$$\|g_j\|^2_{\tilde{H}^{(\sigma,0)}_{\zeta_j}(A_j)} \leqslant \|\chi_j f_1\|^2_{\tilde{H}^\sigma([x_{j-1},x_{j+1}])}\|f_2 - p_2\|^2_{L^2([0,x_{j+1}])} + \|\chi_j(f_1-p_1)\|^2_{\tilde{H}^\sigma([x_{j-1},x_{j+1}])}\|p_2\|^2_{L^2([0,x_{j+1}])} =: B_1 + B_2$$

Let us first consider the term B_1: Interpolation gives

$$\|\chi_j f_1\|_{\tilde{H}^\sigma([x_{j-1},x_{j+1}])} \leqslant c\, h_j^{1/2-\sigma} x_j^{\lambda-\nu}$$

On the other hand we use the one dimensional approximation result

$$\|f_2 - p_2\|_{L^2([0,x_{j+1}])} \leqslant c\left(\frac{x_{j+1}}{j+1}\right)^2 x_{j+1}^{-2\gamma}\|f_2''(x)x^{2\gamma}\|_{L^2([0,x_{j+1}])}$$

With $x_{j+1}/(j+1) \leqslant h_{j+1}$ this implies for $f_2(x) = x^\nu$

$$\|f_2 - p_2\|^2_{L^2([0,x_{j+1}])} \leqslant c\, h_j^4 x_{j+1}^{-4\gamma} x_{j+1}^{2\nu-3+4\gamma}$$

if $2\nu - 4 + 4\gamma > -1$, i.e. $\gamma = 1 - \frac{1}{\beta} > \frac{3-2\nu}{4}$, hence $\beta > \frac{4}{2\nu+1}$. Altogether

$$\sum_{j-2}^{N-1} \|\chi_j f_1\|^2_{\tilde{H}^\sigma([x_{j-1},x_{j+1}])}\|f_2 - p_2\|^2_{L^2([0,x_{j+1}])} \leqslant c' h^{4-2\sigma} \int_0^1 x^{2\lambda-3+(4-2\sigma)\gamma} dx < \infty \qquad (34)$$

for $\sigma < s + \varepsilon$ with ε sufficiently small and $\beta > \frac{2-s}{\lambda+1-s}$.

Next, we consider the term B_2: First we note

$$\|\chi_j(f_1 - p_1)\|^2_{\tilde{H}^\sigma([x_{j-1},x_{j+1}])} \leqslant c\, h_j^{4-2\sigma} h_j x_j^{2(\lambda-\nu-2)}$$

With $f_2(x) = x^\nu$

$$\sum_{j=2}^{N-1} \|\chi_j(f_1 - p_1)\|^2_{\tilde{H}^\sigma([x_{j-1},x_{j+1}])}\|f_2\|^2_{L^2([0,x_{j+1}])} \leqslant C \sum_{j=2}^{N-1} h_j^{5-2\sigma} x_j^{2\lambda-2\nu-4} x_j^{2\nu+1},$$

which one can estimate like (34) above.
Finally, consider g_1 in (33) on A_1. We estimate it by a scaling argument: The square $A_1 = [0,x_2]^2$ is mapped onto $[0,1]^2$ using $\tilde{x} = x_2^{-1}x, \tilde{y} = x_2^{-1}y$, and we write $|g_1(x,y)| = |g_1(x_2\tilde{x}, x_2\tilde{y})| = x_2^\lambda|\tilde{g}(x,y)|$ for $\tilde{g}(x,y) = \tilde{\chi}(x,y)\left(r^\lambda w(\theta) - \tilde{p}\right)$. Here $\tilde{\chi}$, $\tilde{p}$ are independent of h. Interpolation shows that for $\sigma \in [0,1]$

$$\|g_1(x,y)\|_{H^{(\sigma,0)}[0,x_2]^2} \leq x_2^{1-\sigma}\|g_1(x_2\tilde{x}, x_2\tilde{y})\|_{H^{(\sigma,0)}[0,1]^2}$$

and therefore

$$\|g_1(x,y)\|_{H^{(\sigma,0)}[0,x_2]^2} \leqslant C\, x_2^{1-\sigma+\lambda} \leqslant C'\, h^{\beta(1-\sigma+\lambda)}\ .$$

This yields for $\sigma = s + \varepsilon$, $\beta > \frac{2-s}{\lambda+1-s}$ and restriction of $\tilde{A}$ to A for $\tilde{\varepsilon} > 0$ (suff. small)

$$\|f - p\|_{H^{(s+\varepsilon,0)}(A)} \leqslant C\, h^{2-s-\tilde{\varepsilon}}$$

Next, we estimate $f - p$ in $H^{(0,s)}(\tilde{A})$. We subdivide $\tilde{A}$ into disjoint rectangles $\tilde{A}_j = [x_{j-1}, x_j] \times [0, x_{j_0}]$, $j_0 := \min\{j+1, N\}$, $j = 1, \ldots, N$.

In the x-direction only L^2-regularity is used. From Lemma 6.4 we note

$$\|f - p\|^2_{H^{(0,\sigma)}(\tilde{A})} \leqslant \sum_{j=1}^{N} \|f - p\|^2_{H^{(0,\sigma)}(\tilde{A}_j)}$$

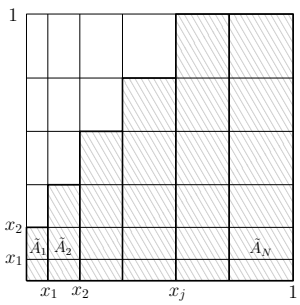

Figure 8: The rectangles $\tilde{A}_j$

for $\sigma \neq \frac{1}{2}$ On the rectangles $\tilde{A}_j (j \geqslant 2)$ we have $f(x,y) = f_1(x)f_2(y), p(x,y) = p_1(x)p_2(y)$. Hence with

$$I_j = [x_{j-1}, x_j], I_j^* = [0, x_{j_0}],\ j_0 = \min\{j+1, N\},\ 0 \leqslant s \leqslant 1 :$$
$$\|f-p\|_{H^{(0,\sigma)}(\tilde{A}_j)} \leqslant \|p_1\|_{L^2(I_j)} \|f_2 - p_2\|_{H^\sigma(I_j^*)} + \|f_1 - p_1\|_{L^2(I_j)} \|f_2\|_{H^\sigma(I_j^*)}$$

Hence it is ea

$$\sum_{j=2}^{N} \|f-p\|^2_{H^{(0,\sigma)}(\tilde{A}_j)} \leqslant c\, h^{4-2\sigma} \sum_{j=2}^{N} h_j x_j^{2\lambda-3+(4-2\sigma)\gamma}\ ,$$

which we already estimated in (34).
The remaining term on $\tilde{A}_1$ can be estimated by the above similarity arguments, leading to

$$\|f-p\|_{H^{(0,\sigma)}(\tilde{A}_1)} \leqslant C\, h^{2-\sigma-\tilde{\varepsilon}}$$

Altogether we have $\|f-p\|_{H^{(0,s+\varepsilon)}(A)} \leqslant c\, h^{2-s-\tilde{\varepsilon}}$, and collecting the estimates obtain with Lemma 6.4 on $Q = A \bigcup B$: $\|f-p\|_{H^{s+\varepsilon}(Q)} \leqslant c\, h^{2-s-\tilde{\varepsilon}}$.

6.4 Approximation of regular edge functions

It remains to address the approximation of the regular edge functions $\tilde{f}(x,y) = \chi(\theta) b(x) y^\nu$, where b is sufficiently smooth and $\chi \equiv 1$ near $\theta = 0$. Due to $b(x) \in H_0^3(I)$ there holds $(1-\chi(\theta))b(x)y^\nu \in H^3(Q)$ and hence it can be approximated like the regular part. We set $f(x,y) = b(x)y^\nu =: f_1(x)f_2(y)$ and $p(x,y) = p_1(x)p_2(y)$ with pw. linear interpolants p_j of f_j. Hence for $0 \leqslant s < \frac{1}{2} + \nu$

$$\begin{aligned}\|f-p\|_{H^s(Q)} \leqslant & \|p_1\|_{L^2(I)} \|f_2 - p_2\|_{H^s(I)} + \|p_1\|_{H^s(I)} \|f_2 - p_2\|_{L^2(I)} \\ & + \|f_1 - p_1\|_{L^2(I)} \|f_2\|_{H^s(I)} + \|f_1 - p_1\|_{H^s(I)} \|f_2\|_{L^2(I)}\ . \end{aligned} \tag{35}$$

We now use the 1D approximation result, Theorem 6.1, to obtain for suitable constants $C > 0$

$$\begin{aligned}\|f_1 - p_1\|_{L^2(I)} &\leq Ch^2 \\ \|f_1 - p_1\|_{H^s(I)} &\leq Ch^{2-s} \\ \|f_2 - p_2\|_{L^2(I)} &\leq Ch^{\min\{\beta(\nu(s)+\frac{1}{2})-\varepsilon, 2\}} \\ \|f_2 - p_2\|_{H^s(I)} &\leq Ch^{\min\{\beta(\nu(s)-s+\frac{1}{2})-\varepsilon, 2-s\}}\ .\end{aligned}$$

Substituting these into (35), we conclude

$$\|f-p\|_{H^s(Q)} \leqslant c\ h^{2-s},$$

for $\beta > \frac{2-s}{\nu+\frac{1}{2}-s}$.

Collecting all the above estimates completes the proof of Theorem 5.2.

7 Numerical approximation of corner exponents

This section discusses the numerical approximation of the generalised eigenvalue problem (16), which determines the corner exponent λ.

Let $\mathsf{b}(u,v)$ be the bilinear form defined in (17), $\mathsf{d}(u,v) = \langle u, v\rangle_H$, where $H = L^2(S^2_+, \cos^{1-2s}(\theta)dS)$. We denote by H_b the closure of $\{u \in C^\infty(S^2_+) : u(\frac{\pi}{2}, \varphi) = 0 \text{ for } \varphi \in (\chi, 2\pi)\}$ with respect to the norm $\|u\|_{H_b} := \mathsf{b}(u,u)^{1/2}$.

Consider the variational formulation of the eigenvalue problem (16):

Find $\mu \in \mathbb{R}$ and $u \in H_b$, nonzero, such that

$$\mathsf{b}(u,v) = \mu\, \mathsf{d}(u,v) \quad \text{for all } v \in H_b. \tag{36}$$

Recall from Lemma 4.2 that (36) admits an orthonormal basis of eigenfunctions $\{\hat{u}_i\}$, with associated eigenvalues $\{\mu_i\}$, so that

$$\mathsf{b}(\hat{u}_i, \hat{u}_j) = \mu_i \mathsf{d}(\hat{u}_i, \hat{u}_j) = \mu_i \delta_{ij}, \quad i,j \in \mathbb{N}. \tag{37}$$

To discretise (36), we consider the finite dimensional subspace $V_h \subset H_b$ of piecewise linear, continuous functions on a triangulation of S^2_+. The discretized eigenvalue problem reads as follows:

Find $\mu_h \in \mathbb{R}$ and $u_h \in V_h$, nonzero, such that

$$\mathsf{b}(u_h, v_h) = \mu_h\, \mathsf{d}(u_h, v_h) \quad \text{for all } v_h \in V_h. \tag{38}$$

Being selfadjoint, the discretized eigenvalue problem (38) admits an orthonormal basis of eigenfunctions $\{\hat{u}_{h,i}\}$, with associated eigenvalues $\{\mu_{h,i}\}$:

$$\mathsf{b}(\hat{u}_{h,i}, \hat{u}_{h,j}) = \mu_{h,i} \mathsf{d}(\hat{u}_{h,i}, \hat{u}_{h,j}) = \mu_{h,i}\delta_{ij}, \quad i,j \in \{1, \dots, \dim(V_h)\}. \tag{39}$$

The following key identity may be found in [6]:

Lemma 7.1. *Suppose that $(\mu, \hat{u})$, $(\mu_h, \hat{u}_h)$ are eigenpairs of the eigenvalue problems (36) and (38), respectively, with $\|\hat{u}\|_H = \|\hat{u}_h\|_H = 1$. Then,*

$$|\mu_h - \mu| = \|\hat{u}_h - \hat{u}\|^2_{H_b} - \mu \|\hat{u}_h - \hat{u}\|^2_H. \tag{40}$$

Proof. Direct computation shows that

$$\begin{aligned}
|\mu_h - \mu| &= \mu_h \mathsf{d}(\hat{u}_h, \hat{u}_h) - \mu \mathsf{d}(\hat{u}_h, \hat{u}_h) \\
&= \mathsf{b}(\hat{u}_h, \hat{u}_h) - \mu \mathsf{d}(\hat{u}_h, \hat{u}_h) \\
&= \mathsf{b}(\hat{u}_h - \hat{u}, \hat{u}_h - \hat{u}) + \mathsf{b}(\hat{u}, \hat{u}_h - \hat{u}) + \mathsf{b}(\hat{u}_h, \hat{u}) - \mu \mathsf{d}(\hat{u}_h, \hat{u}_h) \\
&= \mathsf{b}(\hat{u}_h - \hat{u}, \hat{u}_h - \hat{u}) - \mu \mathsf{d}(\hat{u}_h - \hat{u}, \hat{u}_h - \hat{u}) + \mathsf{b}(\hat{u}_h, \hat{u}) - \mu \mathsf{d}(\hat{u}_h, \hat{u}) \\
&= \mathsf{b}(\hat{u}_h - \hat{u}, \hat{u}_h - \hat{u}) - \mu \mathsf{d}(\hat{u}_h - \hat{u}, \hat{u}_h - \hat{u}) \\
&= \|\hat{u}_h - \hat{u}\|^2_{H_b} - \mu \|\hat{u}_h - \hat{u}\|^2_H.
\end{aligned}$$

□

Graded meshes on the upper hemisphere S^2_+ are β–graded towards the equator as well as the meridians at $\varphi = 0, \chi$, see Figure 10. An example of a 2–graded mesh for $\chi = \pi/3$ is given in Figure 10.

As for Corollary 5.3 the discussion in Section 6 shows that on a β-graded mesh $\|\hat{u}_h - \hat{u}\|_{H_b} \lesssim h^{\min\{\beta\nu(s),\, 2-s\}}$, provided $\beta > \frac{2-s}{\nu(s)+\frac{1}{2}-s}$. We conclude:

Corollary 7.2. *Let μ be an eigenvalue of the eigenvalue problem* (36)*, μ_h the approximate value from the discretized eigenvalue problem* (38)*. For a discretization by a β–graded mesh with $\beta > \frac{2-s}{\nu(s)+\frac{1}{2}-s}$,*

$$|\lambda_h - \lambda| \leq C_{\beta,\varepsilon} h^{2\min\{\beta\nu(s),\, 2-s\}}.$$

For a discretization by a quasi-uniform mesh,

$$|\lambda_h - \lambda| \leq C_{\beta,\varepsilon} h^{2\nu(s)}.$$

Remark 7.3. In addition to the finite element approximation of the spectral problem, analytical approximations of λ prove useful to understand its qualitative behavior, for example the limits $\chi \to 0$ and $\chi \to 2\pi$. An analytical approximation, generalizing results of Noble [28] for mixed boundary problems for the Laplace equation ($s = \frac{1}{2}$), is obtained in the Appendix 10: λ is a solution to the nonlinear equation (54). The different approximations obtained for lambda are illustrated and compared in Section 9.

8 Algorithmic details

We implement the bilinear form a introduced in Section 3 associated with the Dirichlet problem for the integral fractional Laplacian in $\widetilde{\mathbb{V}}_h = \mathbb{S}^1(\mathcal{T}_h) \cap H_0^s(\Omega)$ similarly as described in [2, 3, 23]. In the nodal basis $\{\varphi_i\}$ of $\widetilde{\mathbb{V}}_h$ the stiffness matrix $K = (K_{ij})$ is given by

$$\begin{aligned} K_{ij} = \mathsf{a}(\varphi_i, \varphi_j) = & \frac{c_{n,s}}{2} \iint_{\Omega\times\Omega} \frac{(\varphi_i(x) - \varphi_i(y))(\varphi_j(x) - \varphi_j(y))}{|x-y|^{n+2s}} \,\mathrm{d}y\,\mathrm{d}x \\ & + c_{n,s} \iint_{\Omega\times\Omega^C} \frac{(\varphi_i(x) - \varphi_i(y))(\varphi_j(x) - \varphi_j(y))}{|x-y|^{n+2s}} \,\mathrm{d}y\,\mathrm{d}x\,. \end{aligned}$$

The integrals are computed using a composite graded quadrature as standard in boundary element methods [29, Chapter 5]. This method splits the integral into singular and regular parts. It converts the integral over two elements into an integral over $[0,1]^4$ and resolves the singular part with an appropriate grading. The singular part can be computed explicitly, and for the regular part we employ numerical quadrature. The integrals over Ω^C can be efficiently computed by numerical quadrature after transforming it into polar coordinates.
The computations are carried out on quasi–uniform and β–graded meshes. Graded meshes are designed as discussed in Section 5.

We implement the bilinear form b introduced in (17) associated with the generalised eigenvalue problem (16) on the upper hemisphere S^2_+. In the nodal basis $\{\psi_i\}$ of $\mathbb{V}_h$ the stiffness matrix $A = (A)_{ij}$ is given by

$$A_{ij} = \mathsf{b}(\psi_i, \psi_j) = \int_{S^2_+} \sin(\theta)\cos^{1-2s}(\theta)(\partial_\theta\psi_i)(\partial_\theta\psi_j) + \sin(\theta)^{-1}\cos^{1-2s}(\theta)(\partial_\varphi\psi_i)(\partial_\varphi\psi_j)\ \mathrm{d}\theta\mathrm{d}\varphi\ .$$

Similarly, the mass matrix $M = (M)_{ij}$ is given by

$$M_{ij} = \mathsf{d}(\psi_i, \psi_j) = \int_{S^2_+} \sin(\theta)\cos^{1-2s}(\theta)\psi_i\ \psi_j\ \mathrm{d}\theta\mathrm{d}\varphi\ .$$

For a given discretization on a quasi–uniform or a graded mesh, the eigenvalues of the generalised eigenvalue problem (16) are then computed using the standard MATLAB routine eigs.

9 Numerical experiments

The following numerical experiments illustrate the convergence of finite element approximations on graded meshes, as predicted in Sections 6 and 7. We explore the behavior of the singular exponents ν, λ at the boundary, respectively at a corner, as a function of the fractional order s and the corner angle χ.

Example 9.1. We consider the discretization of the Dirichlet problem (1) as discussed in Section 8 in the L-shaped domain $\Omega = [-1,3]^2 \setminus [1,3]^2 \subset \mathbb{R}^2$ and on triangular domains Ω with an angle χ varied between $\pi/12$ to $5\pi/12$ on uniform and algebraically 2–graded meshes. An example of a 2–graded mesh for the L-shaped domain is depicted in Figure 9 along with a numerical solution for $s = \frac{7}{10}$ on a mesh with 86400 elements.

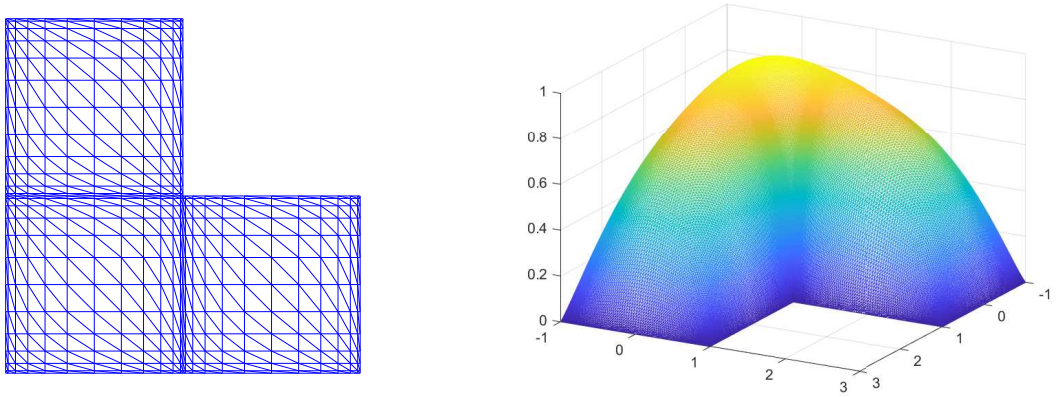

Figure 9: Algebraically 2–graded mesh for L–shaped domain. Numerical solution with $s = \frac{7}{10}$.

Example 9.2. We consider the discretization of the generalised eigenvalue problem (16) employing the bilinear form $\mathsf{b}(u,v)$ discussed in Section 8. As the computational domain we consider the unit upper hemisphere S^2_+ and design quasi–uniform and graded meshes for the opening angle χ. Examples of quasi–uniform and graded meshes are depicted in Figure 10. The shape regularity constant c_R for all meshes is kept $c_R > 3/10$. The meshes are also adjusted around the north pole $\theta = 0$, as shown in the figure.

Figure 10: Examples of a quasi–uniform and graded meshes for the upper hemisphere for $\chi = \pi/3$.

The convergence rates predicted by Corollary 5.3 are illustrated in Figure 11. The figure examines convergence in the energy norm for two distinct values of $s = \frac{1}{2}$ and $s = \frac{7}{10}$, compared to a benchmark solution on a fine 2-graded mesh. The observed rates of convergence for uniform meshes are -0.253 ($s = \frac{1}{2}$) and -0.261 ($s = \frac{7}{10}$). In terms of h, this corresponds to 0.506 ($s = \frac{1}{2}$) and 0.522 ($s = \frac{7}{10}$). For 2-graded meshes we observe rates -0.493 ($s = \frac{1}{2}$) and -0.500 for ($s = \frac{7}{10}$) in terms of DOF, while in terms of h we obtain 0.986 ($s = \frac{1}{2}$) and 1.000 for ($s = \frac{7}{10}$). The rates agree with the theoretical approximation results, which predict an approximation error proportional to $DOF^{-1/2}$ on the 2-graded mesh, and an approximation error proportional to $DOF^{-1/4}$ on a uniform mesh.
Furthermore, the convergence rate of the first eigenvalue for Example 9.2 is presented in Figure 12 for $s = 0.3$ and $s = 0.7$ and the opening angle $\chi = \frac{\pi}{2}$, compared against the benchmark values given in Table 1. The observed convergence rates in the degrees of freedom on uniform meshes are -0.512 ($s = \frac{3}{10}$) and -0.492 ($s = \frac{7}{10}$). In terms of h, this corresponds to a convergence rate of 1.024 ($s = \frac{3}{10}$) and 0.984 ($s = \frac{7}{10}$). Similarly, the convergence rates observed on graded meshes are -0.987 ($s = \frac{3}{10}$) and -1.012 ($s = \frac{7}{10}$), corresponding to 1.974 ($s = \frac{3}{10}$) and 2.024 ($s = \frac{7}{10}$) in terms of h. The rates agree with the theoretical approximation results and are approximately twice the convergence rates for the solutions in the energy norm.

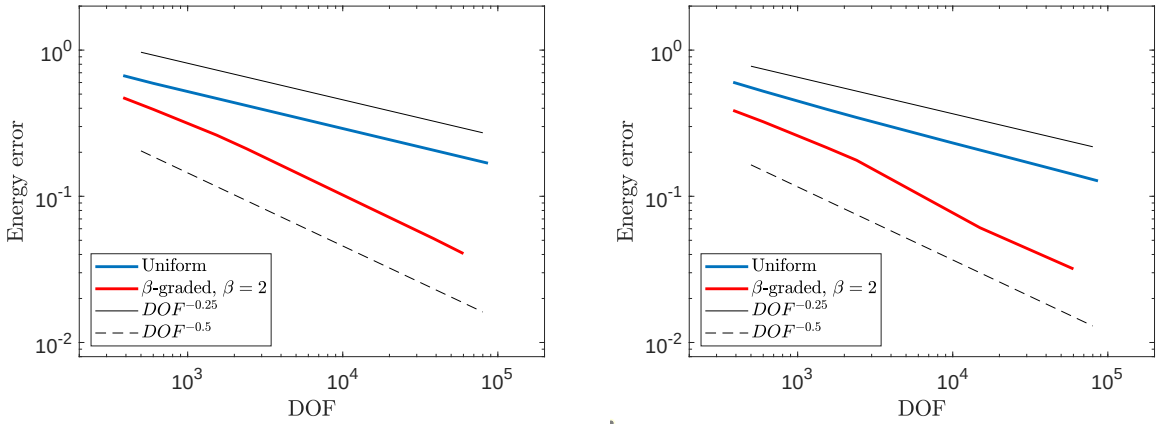

Figure 11: Convergence of the energy norm on a quasi–uniform and 2–graded meshes for $s = \frac{1}{2}$ (left) and $s = \frac{7}{10}$ (right) for Example 9.1.

We compute the singular exponents of the solutions near a corner with opening angle χ by fitting the numerically computed solution to a straight line in a log–log plot. For $s = \frac{1}{2}$ we recover the exponents known for screen problems for the Laplacian [27].

Figures 13 and 14 give examples for the slopes summarized in Table 1. They display the asymptotic behaviour of the solution near corners with angle $\chi = \frac{3\pi}{2}$, $\frac{\pi}{2}$, respectively, for different values of s in a loglog plot on the L-shape depicted in Figure 9. Figure 13 specifically examines the detailed singular behaviour near the re-entrant corner at $(x, y) = (1, 1)$. It shows the solution along cross sections $x = y$, $y = 1$ and $y = 2 - x$. Near the corner, the slope of the solution is approximately 0.297 ($s = \frac{1}{2}$) and 0.44 ($s = \frac{7}{10}$). It is independent of the direction from which the corner is approached, as expected.
Similarly, Figure 14 shows the solution as a function of the distance to three distinct right-angled corners located at $(x, y) = (-1, -1)$, $(3, 1)$, $(3, -1)$. Near the corners, the slope of the solution is approximately 0.815 ($s = \frac{1}{2}$) and 1.17 ($s = \frac{7}{10}$), for all corners.

For completeness, we illustrate the edge behavior in Figure 15. The solution is plotted in a log-log plot near the edge of the domain at $(0, -1)$, where a straight line is expected with slope of the edge exponent $\nu = s$. The numerically observed slopes of the solution near the

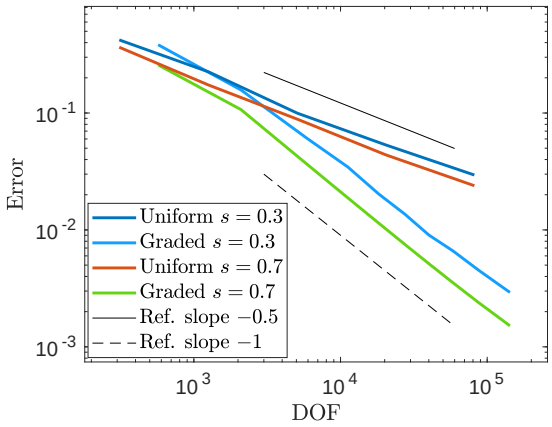

Figure 12: Convergence plot of the first eigenvalue for $s = 0.3$ and 0.7 on uniform and β–graded meshes with $\beta = 2$ with opening angle $\chi = \pi/2$ for Example 9.2.

boundary are 0.498 ($s = \frac{1}{2}$) and 0.697 ($s = \frac{7}{10}$), in good agreement with theory.

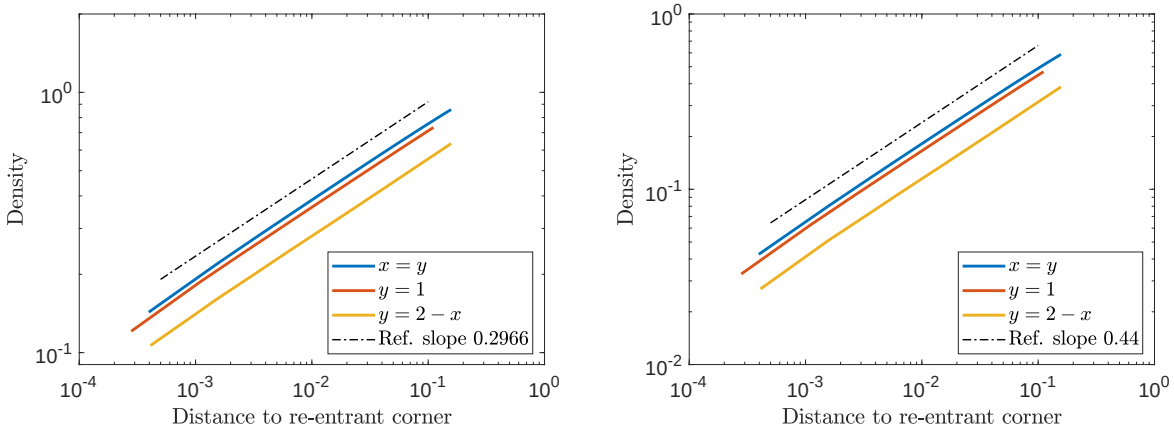

Figure 13: Asymptotic behaviour of the solution near the re-entrant corner for $s = \frac{1}{2}$ (left) and $s = \frac{7}{10}$ (right) in Example 9.1.

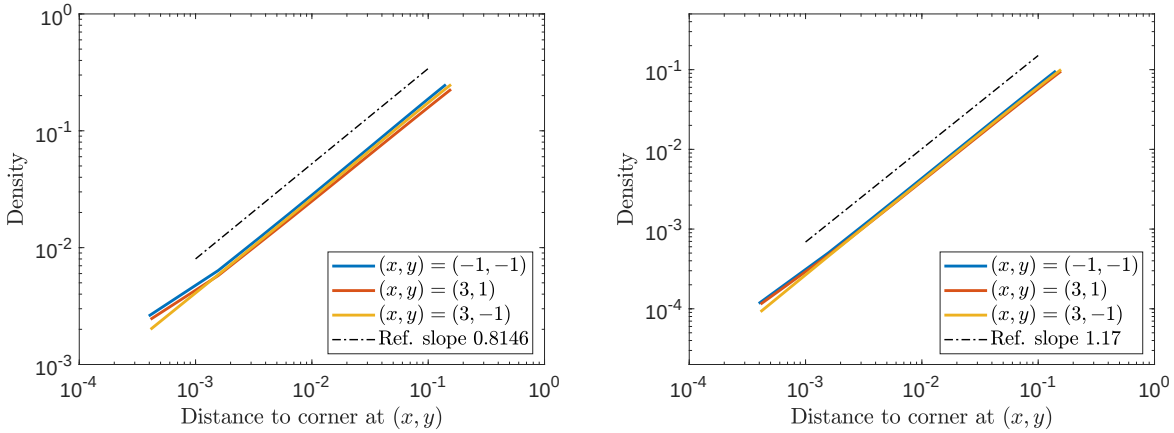

Figure 14: Asymptotic behaviour of the solution near corners at (x, y) for different corners with $s = \frac{1}{2}$ (left) and $s = \frac{7}{10}$ (right) in Example 9.1.

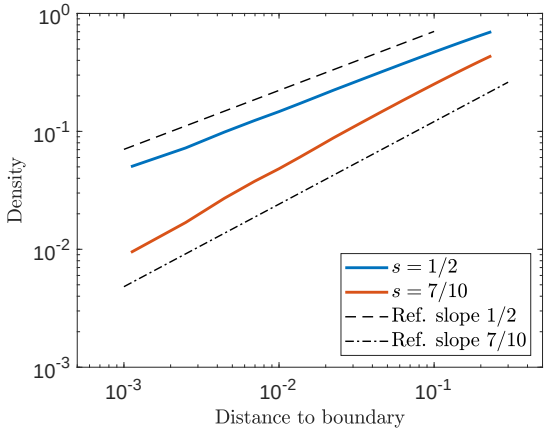

Figure 15: Asymptotic behaviour of the solution near the boundary at $(0, -1)$ for different values of $s = \frac{1}{2}$ and $s = \frac{7}{10}$ in Example 9.1.

More generally, Figure 16 shows the corner exponents as a function of χ for values of s from 0.1 to 0.9 for the values obtained from the numerical solution and from the generalised eigenvalue problem. As expected, the singular exponents decrease as a function of the angle in all cases. We summarise the values of singular exponents for different values of s and the opening angle χ in Table 1 for both the numerical slopes and numerically obtained eigenvalues.

Finally, Figure 17 shows a comparison of the numerically obtained values for the singular exponents using the numerical and eigenvalue problems with the asymptotic expansion presented in Appendix 10. The values are in a good agreement for all three methods. Figure 18 illustrates the corner exponents for the opening angle near $\chi = 2\pi$. It indicates that the singular exponents behave behave like $\max\{0, s - \frac{1}{2}\}$ and demonstrates the sharpness of the lower bound for λ in Corollary 4.4. Curves for the asymptotic expansion are obtained by truncating the sum in (54) at 10^7 terms and using (55) or (56) as an approximation for $R_r(\lambda)$. The deviation for $s \geq 0.8$ may be attributed to these latter approximations.

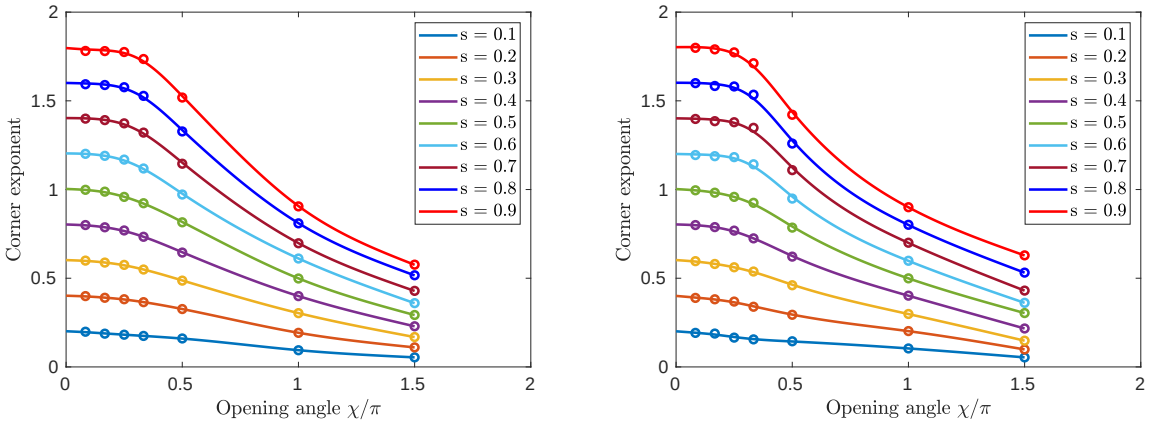

Figure 16: Corner exponents for varied opening angle χ and different values of s obtained from numerical solution of Example 9.1 (left) and the eigenvalue problem of Example 9.2 (right).

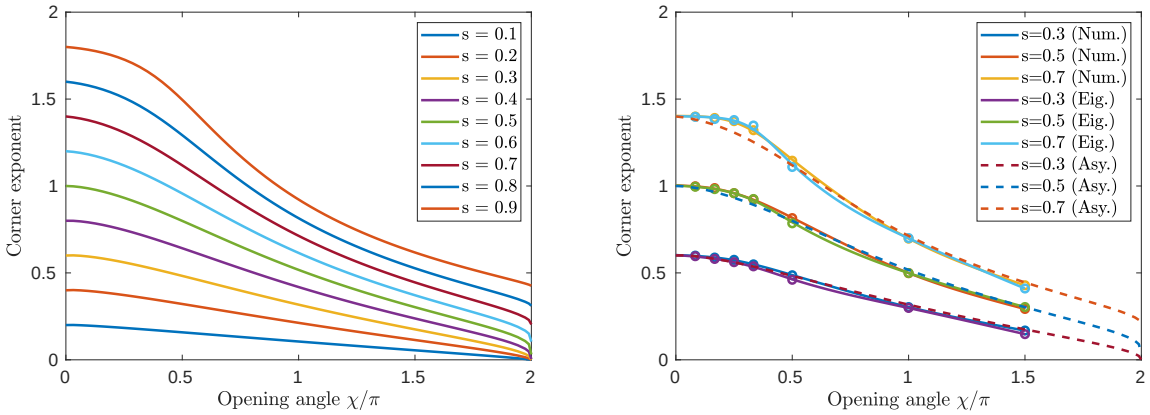

Figure 17: Corner exponents for varied opening angle χ and different values of s obtained from the asymptotic expansion (54) for the solution (left) and comparison of the curves obtained from the numerical solution Example 9.1, the eigenvalue problem Example 9.2, and the asymptotic expansion for different values of s using (54) (right).

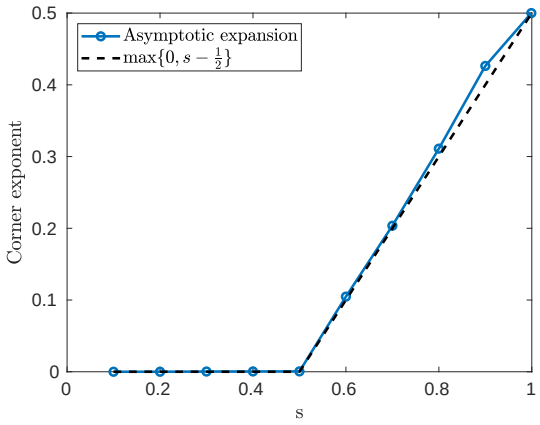

Figure 18: Corner exponents for different values of s from 0.1 until 1 obtained from the asymptotic expansion (54) of the solution at the opening angle $\chi = 2\pi$. The theoretical value $\lambda = \frac{1}{2}$ is used for $s = 1$.

χ/π	1/12		1/6		1/4		1/3		1/2		1		3/2	
s	Num.	Eig.	Num.	Eig.	Num.	Eig.	Num.	Eig.	Num.	Eig.	Num.	Eig.	Num.	Eig.
0.1	0.1984	0.1919	0.1875	0.1881	0.1816	0.1652	0.1748	0.1553	0.1604	0.1446	0.0941	0.1042	0.0540	0.0538
0.2	0.3993	0.3891	0.3898	0.3813	0.3816	0.3684	0.3651	0.3392	0.3263	0.2939	0.1921	0.2021	0.1102	0.0985
0.3	0.5993	0.5962	0.5882	0.5804	0.5752	0.5618	0.5491	0.5378	0.4865	0.4605	0.3032	0.2985	0.1685	0.1478
0.4	0.7998	0.7997	0.7872	0.7882	0.7693	0.7683	0.7336	0.7247	0.6447	0.6218	0.3992	0.4017	0.2292	0.2167
0.5	0.9984	0.9957	0.9880	0.9821	0.9585	0.9586	0.9228	0.9251	0.8153	0.7853	0.4985	0.4993	0.2927	0.3037
0.6	1.2013	1.1944	1.1900	1.1880	1.1687	1.1826	1.1186	1.1423	0.9718	0.9489	0.6111	0.5984	0.3596	0.3613
0.7	1.3996	1.3978	1.3913	1.3853	1.3731	1.3794	1.3209	1.3478	1.1454	1.1093	0.6971	0.7001	0.4288	0.4103
0.8	1.5935	1.5997	1.5891	1.5837	1.5767	1.5810	1.5279	1.5345	1.3274	1.2591	0.8094	0.8012	0.5167	0.5316
0.9	1.7812	1.7988	1.7804	1.7901	1.7752	1.7732	1.7357	1.7119	1.5185	1.4213	0.9050	0.9003	0.5765	0.6289

Table 1: Corner exponents for different values of s and different opening angles χ obtained from the numerical solutions as well as the generalised eigenvalue problem.

References

[1] G. Acosta, F. M. Bersetche, J. P. Borthagaray, *A short FE implementation for a 2d homogeneous Dirichlet problem of a fractional Laplacian*, Computers & Mathematics with Applications 74 (2017), 784-816.

[2] G. Acosta, J. P. Borthagaray, *A fractional Laplace equation: regularity of solutions and finite element approximations*, SIAM Journal on Numerical Analysis 55 (2017), 472-495.

[3] M. Ainsworth, C. Glusa, *Aspects of an adaptive finite element method for the fractional Laplacian: a priori and a posteriori error estimates, efficient implementation and multigrid solver*, Computer Methods in Applied Mechanics and Engineering 327 (2017), 4-35.

[4] I. Babuška, *Finite element method for domains with corners*, Computing 6 (1970), 264-273.

[5] I. Babuška, R. B. Kellogg, J. Pitkäranta, *Direct and inverse error estimates for finite elements with mesh refinements*, Numer. Math. 33 (1979), 447-471.

[6] I. Babuška, J.E. Osborn, *Finite element-Galerkin approximation of the eigenvalues and eigenvectors of selfadjoint problems*, Math. Comp. 52 (1989), no. 186, 275-297.

[7] L. Banjai, J. M. Melenk, R. H. Nochetto, et al., *Tensor FEM for Spectral Fractional Diffusion*, Found. Comput. Math. 19 (2019), 901-962.

[8] L. Caffarelli, L. Silvestre, *An extension problem related to the fractional Laplacian*, Communications in Partial Differential Equations 32 (2007), 1245-1260.

[9] M. Costabel, E. P. Stephan, *Boundary integral equations for mixed boundary value problems in polygonal domains and Galerkin approximation*, Mathematical models and methods in mechanics, 175–251, Banach Center Publ., 15, PWN, Warsaw, 1985.

[10] M. Dauge, *Elliptic boundary value problems in corner domains*, Lecture Notes in Mathematics 1341, Springer Verlag, 1988.

[11] M. D'Elia, M. Gunzburger, *The fractional Laplacian operator on bounded domains as a special case of the nonlocal diffusion operator*, Computers & Mathematics with Applications, 66 (2013), 1245-1260.

[12] E. Di Nezza, G. Palatucci, E. Valdinoci, *Hitchhiker's guide to the fractional Sobolev spaces*, Bulletin des Sciences Mathematiques 136 (2012), 521-573.

[13] Q. Du, *An invitation to nonlocal modeling, analysis and computation*, in: Proceedings of the International Congress of Mathematicians, Rio de Janeiro, 2018, pp. 3523-3552.

[14] G. Estrada-Rodriguez, H. Gimperlein, K. J. Painter, *Fractional Patlak-Keller-Segel equations for chemotactic superdiffusion*, SIAM Journal on Applied Mathematics 78 (2018), 1155-1173.

[15] G. Estrada-Rodriguez, H. Gimperlein, *Interacting particles with Levy strategies: limits of transport equations for swarm robotic systems*, SIAM Journal on Applied Mathematics (2020), to appear.

[16] G. Estrada-Rodriguez, H. Gimperlein, J. Stocek, *Nonlocal interface problems: Modelling, regularity, finite element approximation*, preprint (2019).

[17] H. Gimperlein, N. Louca, R. Mazzeo, in preparation.

[18] H. Gimperlein, J. Stocek, *Space-time adaptive finite elements for nonlocal parabolic variational inequalities*, Computer Methods in Applied Mechanics and Engineering 352 (2019), 137-171.

[19] G. Gilboa, S. Osher, *Nonlocal operators with applications to image processing*, Multiscale Model. Simul. 7 (2009), 1005-1028.

[20] I. S. Gradshteyn and I. M. Ryzhik, *Table of integrals, series, and products (Seventh Edition)*, Elsevier, (2007).

[21] P. Grisvard, *Singular solutions of elliptic boundary value problems in polyhedra*, Portugal. Math. 41 (1984), 367-382.

[22] G. Grubb, *Fractional Laplacians on domains, a development of Hörmander's theory of μ-transmission pseudodifferential operators*, Adv. Math. 268 (2015), 478-528.

[23] J. Gwinner, E. P. Stephan, *Advanced Boundary Element Methods – Treatment of Boundary Value, Transmission and Contact Problems*, Springer Series in Computational Mathematics 52, Springer, 2018.

[24] T. Kato, *Perturbation Theory for Linear Operators*, Springer, 1980.

[25] V. A. Kondratiev, *Boundary value problems for elliptic equations in domains with conic or corner points*, Trans. Moscow. Math. Soc. (1967), 227-313.

[26] V. G. Maz'ya, J. Rossmann, *Elliptic equations in polyhedral domains*, Mathematical Surveys and Monographs, Vol. 162, American Mathematical Society, Providence, RI, 2010.

[27] J. A. Morrison, J. A. Lewis, *Charge Singularity at the Corner of a Flat Plate*, SIAM Journal on Applied Mathematics 31 (1976), 233-250.

[28] B. Noble, *The potential charge distribution near the tip of a flat singular sector*, New York Courant Institute of Mathematical Sciences, 1959.

[29] S. A. Sauter, C. Schwab, *Boundary element methods*, in: Boundary Element Methods, Springer, 2010, 183-287.

[30] T. von Petersdorff, *Randwertprobleme der Elastizitätstheorie für Polyeder-Singularitäten und Approximation mit Randelementmethoden*, Ph.D. thesis, Technische Universität Darmstadt, (1989).

[31] T. von Petersdorff, E. P. Stephan, *Regularity of mixed boundary value problems in $\mathbb{R}^3$ and boundary element methods on graded meshes*, Math. Methods Appl. Sci. 12 (1990), 229-249.

[32] T. von Petersdorff, E. P. Stephan, *Decompositions in edge and corner singularities for the solution of the Dirichlet problem of the Laplacian in a polyhedron*, Math. Nachr. 149 (1990), 71-103.

[33] X. Ros-Oton, J. Serra, *Boundary regularity estimates for nonlocal elliptic equations in C^1 and $C^{1,\alpha}$ domains*, Ann. Mat. Pura Appl. 196 (2017), 1637-1668.

[34] H. Walden, *Solution of an eigenvalue problem for the Laplace operator on a spherical surface*, Goddard Space Flight Center Rep, X-582-74-41, (1974).

[35] P. Wilmott, J. Dewynne, S. Howison, *Option pricing: mathematical models and computation*, Oxford Financial Press, Oxford, 1993.

[36] See *http://functions.wolfram.com/07.23.06.0005.02.*

10 Appendix: Asymptotic Expansion

In the following appendix we derive an analytical approximation th the lowest eigenvalue of the spectral problem (16), and therefore to the corner exponent λ. Our analysis generalises the classical approximation [28] for $s \neq \frac{1}{2}$.

Recall the spectral problem (16), with boundary conditions posed symmetrically around $\varphi = \pi$:

$$\partial_\theta^2 \hat{u} + \frac{1}{\sin^2(\theta)} \partial_\varphi^2 \hat{u} + (\cot(\theta) - (1-2s)\tan(\theta))\, \partial_\theta \hat{u} + \mu^2 \hat{u} = 0,$$

$$\lim_{\theta \to \frac{\pi}{2}^-} \cos^\alpha(\theta) \partial_\theta \hat{\mathrm{u}} = 0 \quad \text{for } \varphi \in \left(\pi - \frac{\chi}{2}, \pi + \frac{\chi}{2}\right),$$

$$\hat{\mathrm{u}} = 0 \quad \text{for } \varphi \notin \left(\pi - \frac{\chi}{2}, \pi + \frac{\chi}{2}\right), \ \theta = \pi/2. \tag{41}$$

The lowest eigenfunction will be even in φ, so that

$$\partial_\varphi \hat{u} = 0, \quad \text{for } \varphi = 0, \pi, \text{ and } \theta \in (0, \pi/2),$$

and the boundary conditions in may be considered only for $\varphi \in \left(\pi - \frac{\chi}{2}, \pi\right)$, respectively $\varphi \in \left(0, \pi - \frac{\chi}{2}\right)$. We look for eigenfunctions to (10) using separation of variables $\hat{u}(\theta, \varphi) = \Phi(\varphi)\ w(\theta)$. We note that Φ satisfies the following equation:

$$\partial_\varphi^2 \Phi = -r^2 \Phi.$$

Then the equation for $w(\theta)$ is given by

$$\partial_\theta^2 w + (\cot(\theta) - (1-2s)\tan(\theta))\, \partial_\theta w + \mu^2 w - \frac{r^2}{\sin^2(\theta)} w = 0. \tag{42}$$

Under the change of variables $z = \sin^2(\theta)$ the above equation becomes

$$z(1-z)\partial_z^2 w + (1 - (2-s)z)\partial_z w + \frac{\mu^2}{4} w - \frac{r^2}{4z} w = 0.$$

We further rewrite the equation using the transformation $w(z) = z^{r/2}\widetilde{w}(z)$:

$$z^{r/2}\left(z(1-z)\partial_z^2\widetilde{w} + ((1+r) - (2+r-s)z)\partial_z\widetilde{w} - \frac{r^2+2r(1-s)-\mu^2}{4}\widetilde{w}\right) = 0. \tag{43}$$

Noting that the expression in the bracket of (43) is the Hypergeometric differential equation, we obtain the general solution $w(z)$:

$$\begin{aligned} w(z) = z^{r/2}\Bigg(&C_1\ {}_2F_1\left(\frac{1-s+r+\sqrt{(1-s)^2+\mu^2}}{2}, \frac{1-s+r-\sqrt{(1-s)^2+\mu^2}}{2}; 1+r; z\right) \\ &+C_2 z^{-r}\,{}_2F_1\left(\frac{1-s-r+\sqrt{(1-s)^2+\mu^2}}{2}, \frac{1-s-r-\sqrt{(1-s)^2+\mu^2}}{2}; 1-r; z\right)\Bigg). \end{aligned}$$

For convenience, we use a transformation for the hypergeometric function [20, Eq. 9.131]:

$${}_2F_1(a,b;c;z) = (1-z)^{c-a-b}\,{}_2F_1(c-a, c-b; c; z),$$

and obtain the following form of the solution:

$$\begin{aligned} w(z) =&C_1(1-z)^s\ z^{r/2}\,{}_2F_1\left(\frac{1+s+r+\sqrt{(1-s)^2+\mu^2}}{2}, \frac{1+s+r-\sqrt{(1-s)^2+\mu^2}}{2}; 1+r; z\right) \\ &+ C_2(1-z)^s z^{-r/2}\,{}_2F_1\left(\frac{1+s-r+\sqrt{(1-s)^2+\mu^2}}{2}, \frac{1+s-r-\sqrt{(1-s)^2+\mu^2}}{2}; 1-r; z\right), \end{aligned}$$

or equivalently, recalling that $\mu^2 = \lambda^2 + (2-2s)\lambda$,

$$\begin{aligned} w(\theta) =&C_1\cos^{2s}(\theta)\ \sin^r(\theta)\,{}_2F_1\left(1+\frac{r+\lambda}{2}, s+\frac{r-\lambda}{2}; 1+r; \sin^2(\theta)\right) \\ &+ C_2\cos^{2s}(\theta)\sin^{-r}(\theta)\,{}_2F_1\left(1-\frac{r-\lambda}{2}, s-\frac{r+\lambda}{2}; 1-r; \sin^2(\theta)\right). \end{aligned} \tag{44}$$

The general solution for $\hat{u}$ is then given by:

$$\hat{u}(\theta,\varphi) = \sum_{r=0}^{\infty} a_r\ w_r(\theta)\cos(r\varphi), \tag{45}$$

where we use $w_r(\theta)$ to highlight the dependency on r.
Application of the boundary conditions (10) to the solution gives:

$$\begin{aligned} \lim_{\theta\to\frac{\pi}{2}-}\sum_{r=0}^{\infty} a_r\ \cos^{\alpha}(\theta)\ \partial_\theta w_r(\theta)\cos(r\varphi) = 0 \quad &\text{for } \varphi\in\left(\pi-\frac{\chi}{2}, \pi\right), \\ \sum_{r=0}^{\infty} a_r\ w_r\left(\frac{\pi}{2}\right)\cos(r\varphi) = 0 \quad &\text{for } \varphi\in\left(0, \pi-\frac{\chi}{2}\right). \end{aligned} \tag{46}$$

The asymptotic expansion of the hypergeometric function ${}_2F_1(a,b;c;z)$ near $z=1$ is given by [36]:

$$\begin{aligned} {}_2F_1(a,b;c;z) \sim&\frac{\Gamma(c)\Gamma(c-a-b)}{\Gamma(c-a)\Gamma(c-b)}\left(1-\frac{ab(z-1)}{1+a+b-c}+\mathcal{O}((z-1)^2)\right) \\ &+\frac{\Gamma(c)\Gamma(a+b-c)}{\Gamma(a)\Gamma(b)}(1-z)^{c-a-b}\left(1+\frac{(a-c)(-b+c)(z-1)}{1-a-b+c}+\mathcal{O}((z-1)^2)\right). \end{aligned} \tag{47}$$

provided that $c-a-b \notin \mathbb{Z}$. We also recall that the derivative of ${}_2F_1(a,b;c;z)$ is given by:

$$\partial_z {}_2F_1(a,b;c;z) = \frac{a\ b}{c} {}_2F_1(a+1,b+1;c+1;z). \tag{48}$$

Thus,

$$\begin{aligned}
&\cos^{1-2s}(\theta)\partial_\theta w_r(\theta) = \\
&C_1\left(-2s\sin^{r+1}(\theta) + r\cos^2(\theta)\sin^{r-1}(\theta)\right) {}_2F_1\left(1+\frac{r+\lambda}{2}, s+\frac{r-\lambda}{2}; 1+r; \sin^2(\theta)\right) \\
&+ C_1\cos^2(\theta)\sin^{r+1}(\theta)\frac{(1+s+r)^2-(\lambda+1-s)^2}{2(1+r)} {}_2F_1\left(2+\frac{r+\lambda}{2}, 1+s+\frac{r-\lambda}{2}; 2+r; \sin^2(\theta)\right) \\
&+ C_2\left(-2s\sin^{-r+1}(\theta) - r\cos^2(\theta)\sin^{-r-1}(\theta)\right) {}_2F_1\left(1-\frac{r-\lambda}{2}, s-\frac{r+\lambda}{2}; 1-r; \sin^2(\theta)\right) \\
&+ C_2\cos^2(\theta)\sin^{-r+1}(\theta)\frac{(1+s-r)^2-(\lambda+1-s)^2}{2(1-r)} {}_2F_1\left(2-\frac{r-\lambda}{2}, 1+s-\frac{r+\lambda}{2}; 2-r; \sin^2(\theta)\right).
\end{aligned} \tag{49}$$

We conclude that $w_r(\theta)$ near $\theta = \frac{\pi}{2}$ is given by

$$w_r(\theta) \sim C_1\frac{\Gamma(1+r)\Gamma(s)}{\Gamma(1+\frac{r+\lambda}{2})\Gamma(s+\frac{r-\lambda}{2})} + C_2\frac{\Gamma(1-r)\Gamma(s)}{\Gamma(1-\frac{r-\lambda}{2})\Gamma(s-\frac{r+\lambda}{2})} + \mathcal{O}\left(\frac{\pi}{2}-\theta\right),$$

and

$$\begin{aligned}
&\cos^{1-2s}(\theta)\partial_\theta w_r(\theta) \sim \\
&C_1\left((-2s)\frac{\Gamma(1+r)\Gamma(s)}{\Gamma(1+\frac{r+\lambda}{2})\Gamma(s+\frac{r-\lambda}{2})} + \frac{(1+s+r)^2-(\lambda+1-s)^2}{2(1+r)}\frac{\Gamma(2+r)\Gamma(1+s)}{\Gamma(2+\frac{r+\lambda}{2})\Gamma(1+s+\frac{r-\lambda}{2})}\right)\left(\frac{\pi}{2}-\theta\right)^{-2s} \\
&C_2\left((-2s)\frac{\Gamma(1-r)\Gamma(s)}{\Gamma(1-\frac{r-\lambda}{2})\Gamma(s-\frac{r+\lambda}{2})} + \frac{(1+s-r)^2-(\lambda+1-s)^2}{2(1-r)}\frac{\Gamma(2-r)\Gamma(1+s)}{\Gamma(2-\frac{r-\lambda}{2})\Gamma(1+s-\frac{r+\lambda}{2})}\right)\left(\frac{\pi}{2}-\theta\right)^{-2s} \\
&+ \left(C_1(-2s)\frac{\Gamma(1+r)\Gamma(-s)}{\Gamma(\frac{r-\lambda}{2})\Gamma(1-s+\frac{r+\lambda}{2})} + C_2(-2s)\frac{\Gamma(1-r)\Gamma(-s)}{\Gamma(-\frac{r+\lambda}{2})\Gamma(1-s-\frac{r-\lambda}{2})}\right) + \mathcal{O}\left(\left(\frac{\pi}{2}-\theta\right)^{2-2s}\right).
\end{aligned} \tag{50}$$

Noting that the prefactors for the singular terms vanish due to the functional equation of the Gamma function, $\Gamma(1+x) = x\Gamma(x)$, the only terms of interest are the constant terms in the third bracket.
For convenience we set

$$\begin{aligned}
Q_1 &= C_1\frac{\Gamma(1+r)\Gamma(s)}{\Gamma(1+\frac{r+\lambda}{2})\Gamma(s+\frac{r-\lambda}{2})} + C_2\frac{\Gamma(1-r)\Gamma(s)}{\Gamma(1-\frac{r-\lambda}{2})\Gamma(s-\frac{r+\lambda}{2})}, \\
Q_2 &= C_1\frac{\Gamma(1+r)\Gamma(1-s)}{\Gamma(\frac{r-\lambda}{2})\Gamma(1-s+\frac{r+\lambda}{2})} + C_2\frac{\Gamma(1-r)\Gamma(1-s)}{\Gamma(-\frac{r+\lambda}{2})\Gamma(1-s-\frac{r-\lambda}{2})}.
\end{aligned}$$

Furthermore, let $b_r = a_r Q_2$ and $R_r(\lambda) = Q_1/Q_2$. Then we write the boundary conditions from (46) as

$$\begin{aligned}
\sum_{r=0}^{\infty} b_r\cos(r\varphi) = 0 \quad &\text{for } \varphi \in \left(\pi-\frac{\chi}{2}, \pi\right), \\
\sum_{r=0}^{\infty} b_r R_r(\lambda)\cos(r\varphi) = 0 \quad &\text{for } \varphi \in \left(0, \pi-\frac{\chi}{2}\right).
\end{aligned} \tag{51}$$

The quantity $R_r(\lambda)$ can be further simplified:

$$\begin{aligned}
R_r(\lambda) &= \frac{\Gamma(s)}{\Gamma(1-s)} \frac{C_1 \frac{\Gamma(1+r)}{\Gamma(1-r)\Gamma(1+\frac{r+\lambda}{2})\Gamma(s+\frac{r-\lambda}{2})} + C_2 \frac{1}{\Gamma(1-\frac{r-\lambda}{2})\Gamma(s-\frac{r+\lambda}{2})}}{C_1 \frac{\Gamma(1+r)}{\Gamma(1-r)\Gamma(\frac{r-\lambda}{2})\Gamma(1-s+\frac{r+\lambda}{2})} + C_2 \frac{1}{\Gamma(-\frac{r+\lambda}{2})\Gamma(1-s-\frac{r-\lambda}{2})}} \\
&= \frac{\Gamma(s)}{\Gamma(1-s)} \frac{\frac{1}{\Gamma(1-\frac{r-\lambda}{2})\Gamma(s-\frac{r+\lambda}{2})}}{\frac{1}{\Gamma(-\frac{r+\lambda}{2})\Gamma(1-s-\frac{r-\lambda}{2})}} \\
&= \frac{\Gamma(s)}{\Gamma(1-s)} \frac{\Gamma(-\frac{r+\lambda}{2})\Gamma(1-s-\frac{r-\lambda}{2})}{\Gamma(1-\frac{r-\lambda}{2})\Gamma(s-\frac{r+\lambda}{2})} \\
&= \frac{\Gamma(s)}{\Gamma(1-s)} \frac{\Gamma(\frac{r-\lambda}{2})\Gamma(1-s+\frac{r+\lambda}{2})}{\Gamma(1+\frac{r+\lambda}{2})\Gamma(s+\frac{r-\lambda}{2})},
\end{aligned}$$

where we used the fact that $\frac{\Gamma(1+r)}{\Gamma(1-r)} = 0$ for $r \in \mathbb{N}$ and repeatedly used of $\Gamma(1+x) = x\Gamma(x)$. We then rewrite (51) as

$$\begin{aligned}
b_0 + \sum_{r=1}^{\infty} b_r \cos(r\varphi) = 0 \quad \text{for } \varphi \in \left(\pi - \frac{\chi}{2}, \pi\right), \\
R_0(\lambda) b_0 + \sum_{r=1}^{\infty} b_r R_r(\lambda) \cos(r\varphi) = 0 \quad \text{for } \varphi \in \left(0, \pi - \frac{\chi}{2}\right).
\end{aligned} \tag{52}$$

Suppose that the first equation of (52) equals to an unknown function $f(\varphi)$. The coefficients b_r are given by

$$\begin{aligned}
b_0 &= \int_0^{\pi-\chi/2} f(u)\mathrm{d}u, \\
b_r &= 2\int_0^{\pi-\chi/2} f(u)\cos(ru)\mathrm{d}u.
\end{aligned}$$

Then (52) becomes

$$R_0(\lambda) \int_0^{\pi-\chi/2} f(u)\mathrm{d}u + 2\sum_{r=1}^{\infty} R_r(\lambda) \int_0^{\pi-\chi/2} f(u)\cos(ru)\mathrm{d}u \cos(r\varphi) = 0. \tag{53}$$

We seek a function that has a correct behaviour near $\varphi = \pi \pm \frac{\chi}{2}$. One possibility is to choose

$$f(u) = \left(1 - \left(\frac{u}{\pi - \frac{\chi}{2}}\right)^2\right)^{s-1}.$$

Note that for such choice of $f(u)$ the integrals in (53) are explicitly computable.

$$\begin{aligned}
\int_0^{\pi-\chi/2} f(u)\mathrm{d}u &= \frac{(2\pi-\chi)\sqrt{\pi}\Gamma(s)}{4\Gamma(s+\frac{1}{2})}, \\
\int_0^{\pi-\chi/2} f(u)\cos(ru)\mathrm{d}u &= \frac{(2\pi-\chi)\sqrt{\pi}\Gamma(s)}{4} \left(\frac{(2\pi-\chi)r}{4}\right)^{\frac{1}{2}-s} J_{s-\frac{1}{2}}\left(\frac{(2\pi-\chi)r}{2}\right),
\end{aligned}$$

where $J_s(z)$ is Bessel function of the first kind. We further integrate the expression in φ and obtain a transcendental equation for λ:

$$R_0(\lambda) + \frac{8}{2\pi-\chi} \sum_{r=1}^{\infty} \frac{\sin\left(\frac{(2\pi-\chi)r}{2}\right)}{r} R_r(\lambda)\Gamma\left(s+\frac{1}{2}\right) \left(\frac{(2\pi-\chi)r}{4}\right)^{\frac{1}{2}-s} J_{s-\frac{1}{2}}\left(\frac{(2\pi-\chi)r}{2}\right) = 0. \tag{54}$$

For $\lambda = 0$ we obtain:

$$R_r(0) = \frac{2\Gamma(s)\Gamma(1-s+\frac{r}{2})}{r\Gamma(1-s)\Gamma(s+\frac{r}{2})}. \tag{55}$$

Alternatively, for $\lambda = s - \frac{1}{2}$ we obtain:

$$R_r\left(s-\frac{1}{2}\right) = 2^{2s}\frac{\Gamma(s)\Gamma\left(\frac{1}{2}+r-s\right)}{\Gamma(1-s)\Gamma\left(\frac{1}{2}+r+s\right)}. \tag{56}$$

Since analysis in Corollary 4.4 establishes that $\lambda \geq \max\left(0, s-\frac{1}{2}\right)$, we will use one of these quantities as an approximation for $R_r(\lambda)$ for all λ. Equation (54) can be approximated numerically by truncation of the series and using (55) or (56) for $r = 1, 2, 3, \ldots$.
We compare the approximate results of (54) with the corner exponents obtained by numerical approximation as well as the generalised eigenvalue problem.

Remark 10.1. Note that for $\chi \to 0$ the equation (54) reduces to:

$$\frac{\Gamma(-\frac{\lambda}{2})\Gamma(1-s+\frac{\lambda}{2})}{\Gamma(1+\frac{\lambda}{2})\Gamma(s-\frac{\lambda}{2})} = 0.$$

This equation is satisfied when $\lambda = 2s$.